Sensors and Actuators Reports 4 (2022) 100098

Contents lists available at ScienceDirect

Sensors and Actuators Reports

journal homepage: www.sciencedirect.com/journal/sensors-and-actuators-reports

ZnO nano-structured based devices for chemical and optical sensing applications

Rinky Sha [a,1,*], Arindam Basak [b,1], Palash Chandra Maity [c], Sushmee Badhulika [d]

[a] Sensors for Health-care and Environmental monitoring (SHE) Lab, Department of Electronics and Communications Engineering, Indian Institute of Information Technology, Kalyani, West Bengal 741235, India
[b] Thin Film Photovoltaic Lab, School of Electronics Engineering, KIIT- Deemed to be University, Bhubaneswar 751024, Odisha, India
[c] Department of Metallurgical and Materials Engineering, Indian Institute of Technology Roorkee, Roorkee, Uttarakhand 247667, India
[d] Department of Electrical Engineering, Indian Institute of Technology Hyderabad, Hyderabad 502285, India

ARTICLE INFO

Keywords:
ZnO
Sensors
Biomedical
Environmental monitoring
Solar cell
Photodetector

ABSTRACT

Zinc oxide (ZnO), a direct, wide band gap and n-type metal oxide semiconductor, is being anticipated as the next generation functional nano-material towards remarkably diversified sensing applications. ZnO and its composites have revealed a new era in the fabrication of sensors owing to their excellent opto-electronic, physicochemical, electrical properties such as low dielectric constant, plentiful Zn-O bonds, high luminous transmittance, good physicochemical stability, huge excitation binding energy, non-toxicity, biocompatibility, large surface area to volume ratio and so on. This comprehensive review summarizes the applications of ZnO nano-structures in the areas of environmental monitoring, biomedical, and optical sensing. Fundamental sensing mechanisms of the ZnO based sensors are examined to provide a better insight into the role of ZnO in each of these sensors. Wherever relevant, limitations of the existing approaches and future outlook have also been discussed.

1. Introduction

Recognition of analytes such as biomolecules, pollutants, explosives, heavy metal ions etc. is important in improving the superiority of human life in terms of disease identification-management and environmental protection. This has steered to the scientists to stress upon developing the cost-effective sensors with good sensitivity, selectivity, reproducibility, low detection limit, and long-term durability. A sensor is an analytic device that quantitatively or semi-quantitatively transforms the information about the presence of a physical (like gas, temperature, light intensity) or chemical species (analyte) to a computable signal. Its functioning contains two important stages: (a) recognition and (b) transduction. In the course of recognition, the analyte interacts with the receptor molecules or the active sites involved in the structure of the recognition element of the sensor while the transducer translates this event into a suitable signal like resistance, potential or current [1–4]. In past decades, several nano-materials like metal and metal oxide semiconductors based sensors [5–10] have been affirmed to meet the rising demand of the bio/chemical sensors in numerous arenas such as clinical, food safety, environmental monitoring etc.

On the other side, solar energy, a gift of nature in different forms and phases, is gaining interest among the research community with the development of different several technologies. One major application to utilize solar energy is the photovoltaic cells [11]. Photovoltaic cells, in its different form of structure are researched extensively to obtain better efficiency at an optimum condition. Although high efficiency can be achieved with Si based solar cell, but the availability of high quality Si single crystals is quite difficult which in turn reduces its application potential and increases the cost. So, to reduce the cost poly-Si or amorphous-Si, CIGS, CdTe are solar cell were extensively researched [12]. Though the efficiency obtained by these types of solar cell was less in comparison to conventional Si solar cell, but their application as an absorber in the solar cell opens a new era of research along with the exploration of the potential of different nanostructure like nanowires, nanotubes, nanoparticles etc. [13]. Also different types of solar cell like homo or hetero junction, dye sensitized, perovskite are widely researched to find the optimum device parameters and to enhance the photovoltaic performance [14–15]. Among them perovskite and dye-sensitized solar cell are now gaining interest among the researchers due to their high photovoltaic performance, low fabrication cost and

* Corresponding author.
E-mail address: rinky@iiitkalyani.ac.in (R. Sha).
[1] Equal contribution.

https://doi.org/10.1016/j.snr.2022.100098
Received 2 November 2021; Received in revised form 22 February 2022; Accepted 28 March 2022
Available online 3 April 2022

abundance. Perovskite solar cell (PSCs) consists of mainly a metal oxide layer with a perovskite sensitized material, a hole transport layer and a metal electrode. Oxide layer plays a significant role in determining the efficiency of the solar cell, whereas the oxide layers are used for creating effective path for charge generation, carrier transport and utilizing high surface area for dye absorption. A careful design and deposition of oxide material with high mobility are very important to obtain a solar cell with high efficiency. Alternatively, photo-detector is another type of photo sensing device which converts the incident light into electrical signal where the sensitivity of the detector is a major determining factor while evaluating the device performance. UV light sensing is widely associated with our daily life including missile, optical communication, and biomedical applications [16]. Hence, there is an urgent need towards development of the photodetectors.

Nanotechnology has appeared as one of the most exciting forefront fields. Diversity of nano-materials of numerous morphologies, chemical compositions with the prerequisite surface properties, crystalinity and so on had steered to their usage in the chemical and optical sensing applications [17–19]. In this aspect, semiconducting metal oxides such as Zinc oxide (ZnO), has engrossed significant consideration as a next age-band functional nano-material for sensing applications due to their brilliant electronic, physico-chemical, catalytic and optical properties [20–21]. ZnO, a direct, wide band gap (3.37 eV) and n-type semiconductor shows excellent properties like plentiful Zn-O bonds, low price, low dielectric constant, high luminous transmittance, good physicochemical stability, huge excitation binding energy (60 meV), non-toxicity, good piezoelectric property, biocompatibility, high electron mobility, large surface area to volume ratio [22–25]. Apart from the above applications, ZnO can also be used as a main constituent element for sunscreen and different healing ointments due to it's anti-microbial and UV light absorbing properties. With the rapid development in the technology, different nano structures developed for ZnO, can be used in different applications where specific porosity, roughness, size and morphology is required. All the above properties described above mainly depends on the deposition properties like the elements present on the solution, pH of the solution, temperature of the deposition environment and aggregation tendency [26]. ZnO reveals two phases, (a) hexagonal wurtzite and (b) cubic zinc blende phase. Among these two phases, the wurtzite phase is more stable at ambient conditions and provides ease in the growth of ZnO with the adaptable morphologies. The tetrahedral coordination of the atoms in the wurtzite directs to non-centro symmetric crystal structure with Zn^{2+} and O^{2-} polar surfaces resulting in piezoelectric properties that help to employ these nanostructures in mechanical actuators, sensing devices. Bulk ZnO possesses high Young's modulus of ~ 150 GPa and admirable temperature stability upto ~1800°C [27–28]. Another suitable application of ZnO nanostructures is photo detector, mainly for the sensing of UV lights due to its preferable opto-electronic properties like wide band gap, high binding energy, photo absorption in UV range, and high surface area to volume ratio. Also by using ZnO nanostructures and after doping with different materials, the photocurrent can be improved, which in turn improves the sensitivity of the detector [29–30].

So far, various methods like hydrothermal, solvothermal, sol–gel, co-precipitation, solid-state, combustion, electro-spinning, template-assisted growth, chemical vapor deposition etc. have been established towards the synthesis of ZnO nanostructures. Every synthesis route has its own benefits and intrinsic restrictions. Most of these synthesis approaches include surfactants or templates for the preparation of ZnO nanostructures. Elimination of organics from the nano-structures is a major issue and affects the reproducibility of analysis while the physical vapor methods, like RF and DC sputtering, enable the possibility of engineering 3D hierarchical ZnO structures without the use of surfactants or template [31–32].

This review delivers a compact knowledge on the applications of ZnO nano-structures in the area of biomedical, environmental and optical sensing concurrently. Fundamental sensing mechanisms of the ZnO nano-structure are systematically conferred to provide better insight into how ZnO ascribed in each sensor. Also, the limitations and the ways to improve the sensitivity of ZnO nano-structures as different types of sensors are described in an elaborated manner. This will facilitate the research communities to have a better overview about the potential of ZnO nano-structures, its diverse application as different types of sensors.

2. Applications of ZnO nano-structured based devices for chemical sensing

2.1. Biomedical applications

Biomolecules such as glucose, urea, dopamine (DA), ascorbic acid (AA), uric acid (UA), hydrogen peroxide (H_2O_2), DNA, proteins like myoglobin (Mb), troponin, cancer antigen 125, prostate specific antigen (PSA) etc. play an important role in several disease developments; e.g., excessive level of UA in the blood has been related to arthritis, heavy hepatitis, gout, neurological, and renal diseases whereas DNA damage causes the risk of Alzheimer's and cancer [33–38]. Hence, early recognition of these biomolecules is of utmost significance in disease identification along with treatment. Because of remarkable physico-chemical, electronic, photochemical properties like biocompatibility, non-toxicity, huge specific surface area, quick electron transfer rate, and chemical stability, ZnO based nanomaterials have been broadly utilized as a sensing material towards the fabrication of various sensors [33,39].

2.1.1. Recognition of glucose

Checking of glucose levels in human blood, tear, urine, and/ or saliva is essential for diagnosis and controlling of diabetes mellitus. Determination of glucose can be realized by using glucose oxidase (GOx) enzyme as a recognition element [3,40-41]. ***Baruah et al.*** [42] demonstrated the Co-Fe doped ZnO based electrode for the enzymatic sensing of glucose where this composite was prepared via the hydrothermal method. In enzymatic glucose sensor, recognition was done through the production of H_2O_2 resulting from the redox reactions of GOx. The GOx modified Co-Fe doped ZnO sensor showed almost two folds greater sensitivity (32.2 μA mM^{-1} cm^{-2}) than only ZnO based sensor over the linear range of 0-4 mM of glucose with detection limit of 0.27 mM, acceptable selectivity over cholesterol, UA and response time of 6.21 s. This enhanced performance of the composite based biosensor was ascribed to an enhanced electro-active surface area for loading of enzyme originating from the reduced crystallite size of the composite, improved charge transfer kinetics resulting from the presence of defect states into ZnO band-gap. ***Anusha et al.*** [43] developed the chitosan (CS)-Pt NPs decorated porous ZnO nanostructure based enzymatic sensor for glucose detection. The GOx immobilized ZnO-Pt-CS based biosensor showed a good sensitivity of 62.14 μA mM^{-1} cm^{-2} and limit of detection (LoD) of 16.6 μM over the linear range of 100 μM – 2 mM of glucose. GOx was encapsulated within the CS, partly based on electrostatic interaction between the positively charged CS and negatively charged GOx with enhanced catalytic properties. ***Ridhuan et al.*** [44] presented the Pt nanodendrites decorated ZnO nanorods for enzymatic glucose sensor where the Pt nanodendrites with an average size of ~ 40 nm were prepared by the chemical reduction technique. The GOx immobilized composite based biosensor displayed a sensitivity of 98.34 μA mM^{-1} cm^{-2} over the linear range of 0.05–1 mM glucose with low detection limit of 30 μM, decent stability of 1 month and specificity over uric acid and ascorbic acid. The sensor was validated through detection of glucose in real human blood samples. ***Yang et al.*** [45] reported the Cu-ZnO nano-thorn array for non-enzymatic, photoelectrochemical sensing of glucose in neutral solution. This sensor revealed good photo-activity, good sensitivity of 63.76 μA mM^{-1} cm^{-2} over the linear range of 0.1–4.5 mM, with a limit detection of 3.762 μM, decent stability of 16 days, repeatability and selectivity over DA, AA and UA. The practicality of this sensor was assessed through detection of glucose in human serum samples. The excellent performance of this electrode was ascribed to

good conductivity and high electro- active area of Cu-ZnO composite. Furthermore, the Schottky junction was formed between the trunk of Cu nanorods and the branches of ZnO nanowires, thus easing the separation of photo-generated electrons and holes. ***Awais et al.*** [46] described the vertically aligned Au-ZnO nanorods based non-enzymatic glucose sensor. This glucose sensor showed a high sensitivity of 4416 μA mM^{-1} cm^{-2} over the linear region of 0.001–15 mM, with a limit detection of 0.12 μM, satisfactory stability of 15 days, reproducibility and good specificity over DA, CA, fructose, AA and UA. The applicability of this sensor was evaluated through detection of glucose in human blood samples. The distinctive hexagonal Au-ZnO nanorods with enhanced surface area improved the electrochemical properties towards glucose oxidation. ***Vinoth et al.*** [47] demonstrated the ZnO quantum dots with ~ 3–8 nm diameters supported multi-walled carbon nanotubes (MWCNTs) based electrode for non-enzymatic glucose sensing. The ZnO quantum dots -MWCNTs composite based sensor exhibited have a sensitivity of 9.36 μA μM^{-1} over the dynamic range of 0.1 - 2.5 μM glucose with good repeatability, low detection limit of 0.208 μM, fast response time (< 3 s), good stability of 30 days and selectivity over sucrose, AA, DA and UA. This developed sensor was effectively used to sense glucose in human urine samples with recovery% of 98-102.1%. ***Imran et al.*** [48] developed the graphitic carbon nitride (g-C_3N_4)-Pt-ZnO composite for non-enzymatic recognition of glucose where the Pt- g-C_3N_4 was synthesized by the pyrolysis technique. Glucose was sensed via oxidation at a low potential of +0.20 V (vs. Ag/AgCl). The sensor exhibited a sensitivity of 3.34 μA mM^{-1} cm^{-2} over the dynamic range of 0.25–110 mM glucose with good repeatability, low detection limit of 0.1 μM, rapid response time (5 s), good stability of 60 days and selectivity over fructose, galactose, riboflavin, bilirubin, biotin, NaCl, KCl, H_2O_2, UA, serotonin and epinephrine. The fabricated sensor was assessed in human blood, serum and urine samples. This economical sensor was 4 time reusable in whole blood without deterioration in its activity. ***Manna et al.*** [49] presented the Cu_2O-ZnO composite based non-enzymatic glucose sensor where the composite was synthesized by the one-step co-electrodeposition method. This sensor displayed a good sensitivity of 441.2 μA mM^{-1} cm^{-2} over the linear range of 0.02–1 mM glucose with a detection limit of 0.13 μM, fast response time (< 3 s), acceptable specificity over AA, DA, UA, good reproducibility and stability of 34 days. This excellent performance was due to direct electron transfer between the active sites and the electrode resulting from its conjugated nanostructures. ***Zhou et al.*** [50] reported the hexagonal structured ZnO nanorods modified flexible non-enzymatic electrochemical sensor for recognition of glucose where the ZnO nanorods were hydrothermally grown on bendable stainless steel wire sieve electrode. The electro-catalytic properties of the sensor towards glucose were visibly boosted with ultraviolet treatment introduced in the course of the sensing experiments as it endorses the generation of holes in the ZnO nanorods, thus increasing the amount of hydroxyl. Consequently, more hydroxyl reacts with glucose and further the electron yield of the glucose sensor is notably increased, thus the sensitivity of the glucose sensor is raised from 36.4 μA mM^{-1} cm^{-2} to 91.8 μA mM^{-1} cm^{-2}. Moreover, this sensor exhibited good sensitivity with excellent specificity towards other common interfering biomolecules such as d-galactose, fructose, urea, UA, AA, l-phenylalanine, NaCl, and KCl. Validation was done through successful detection of glucose concentrations in human serum samples. ***Waqas et al.*** [51] demonstrated the 3D $Ni(OH)_2$ nanosheet - coated marigold-like ZnO microflower (mg-ZnO@$Ni(OH)_2$ NSs) composite for the non-enzymatic sensing of glucose wherein this composite was prepared by a one-pot solvothermal route. This sensor exhibited a high sensitivity,low limit of detection of 0.06 μM with good stability and selectivity. This sensor was validated via successful detection of glucose in human serum samples.

2.1.2. Recognition of urea

Urea, an organic compound is one of the ending products of protein metabolism. Sensing of urea is vital in biomedical arena because its timely recognition benefits us to avoid numerous hepatic and kidney diseases [52]. Determination of urea can be realized by using urease enzyme as a recognition element. ***Ahmad et al.*** [53] reported the directly grown vertically aligned ZnO nanorods on the Ag sputtered glass substrate for the enzymatic urea sensing where ZnO nanorods were grown via a low temperature solution method. The urease immobilized ZnO nanorods based sensor showed a great sensitivity of 41.64 μA mM^{-1} cm^{-2} over the wide linear region of 0.001–24 mM urea, with a low detection limit of 10 μM, stability of 20 weeks and satisfactory selectivity over glucose, UA, cholesterol and AA. This improved performance of the biosensor was attributed to high specific surface area, thus offering high enzyme loading and improved sensor efficacy. But this biosensor was not validated for practical applications. ***Rahmanian et al.*** [54] described a disposable urea biosensor based on the nanoporous ZnO film fabricated from omissible polymeric substrate, polyvinyl alcohol (PVA).The sensor showed a high sensitivity of 0.0506 kΩ per mg dL^{-1} for urea detection over the range of 8.0–110.0 mg dL^{-1} with the limit of detection of 5 mg dL^{-1}, rapid response time (<10 s) and storage stability of 5 weeks. This developed sensor was used to sense urea in serum samples. ***Babitha et al.*** [55] demonstrated the ZnO- reduced graphene oxide (rGO) composite for the non-enzymatic sensing of urea wherein the composite was synthesized by a green synthetic route via a sequence of bio-templates like dextrose, sucrose, soluble starch, and carboxy methyl cellulose. This sensor revealed an excellent sensitivity of 682.8 μA mM^{-1} cm^{-2} towards urea over the concentration range of 0.02 - 7.2 μM with a detection limit of 0.012 μM. But this sensor was not authenticated for practical applications. ***Yoon et al.*** [56] developed the Ag-ZnO nanostructures based C electrode for non-enzymatic recognition of urea wherein the Ag-ZnO nanorods and nanoflakes with various crystallographic orientations were prepared by a combination of sputter deposition and solution growth method as depicted in **Fig. 1 (a-c)**. **Fig. 1 (d)** displays the amperometric responses of the Ag-ZnO nanorods/carbon paper and Ag-ZnO nanoflakes/carbon paper electrodes at different potential from 0.35 - 0.70 V vs. Ag/AgCl on in the absence and presence of 0.33 M urea in 1 M KOH of electrolyte. The Ag-ZnO nanorods/carbon paper electrode exhibited a higher current density (12 mA cm^{-2} mg^{-1}) than the Ag-ZnO nanoflakes/carbon paper electrode at all potentials which was due to higher surface area (169 cm^2 mg^{-1}), thus offering higher current densities towards electro-oxidation of urea at very low onset voltage of 0.41 V vs. Ag/AgCl. ***Kushwaha et al.*** [57] presented the ZnO encapsulated polyaniline-grafted CS composite for potentiometric urea sensor. This sensor exhibited a sensitivity of 187.5 μV ppm^{-1} cm^{-2} over concentration range of 20 - 500 ppm or 0.3 - 8.3 mM with a low detection limit of 29.84 ppm, good stability of 8 weeks, specificity over glucose, UA, AA, lactic acid and cholesterol. This developed sensor was validated through detection of urea in human blood serum samples.

2.1.3. Recognition of DA

Sensing of DA levels is important in clinical diagnostics as it is a vital excitatory neurotransmitter released by the brain. Its unusual levels roots the progression of a number of neurological diseases including Alzheimer's, Parkinson's, and Huntington's disease, schizophrenia, drug addiction etc. Detection of DA can be realized by using tyrosinase enzyme as a recognition element [58]. ***Zhihua et al.*** [59] reported the carbon-ZnO microfiber for dopamine sensing in pork wherein the composite was prepared using the hypha of Penicillium expansum as economical and green template. The coaxial structure was formed via the attachment of Zn^{2+} on the surface of hypha through coordination and electrostatic interactions. This sensor revealed good selectivity over AA and 5-hydroxytryptamine, reproducibility, and stability of 1 month with a detection limit of 0.106 μM. Two linear ranges were achieved from 0 - 50 and 50 - 300 μM. The applicability of the carbon-ZnO microfibers based sensor was examined by the fruitful detection of DA in pork with recovery% of 96.85% -104.51%. ***Li et al.*** [60] described the ZnO nanorods-rGO composite based DA sensor where this composite

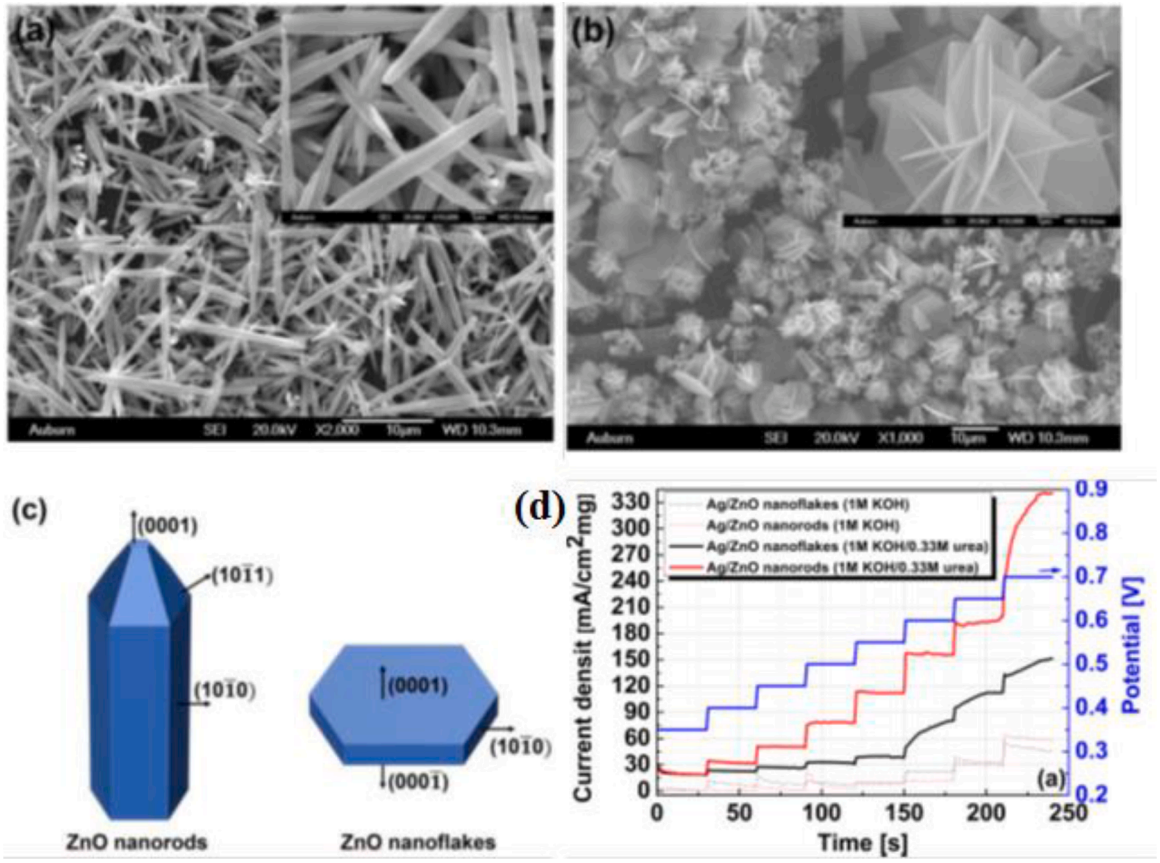

Fig. 1. SEM images of (a) ZnO nanorods and (b) ZnO nanoflakes, and diagram of obelisk shaped (c) ZnO nanostructures, (d) Amperometric responses at different potential from 0.35 to 0.70 V vs. Ag/AgCl on Ag-ZnO nanorods/carbon paper and Ag-ZnO nanoflakes/carbon paper electrodes in the absence and presence of 0.33 M urea in 1 M KOH of electrolyte. Reprinted with permission from [56].

was prepared via hydrothermal treatment followed by an electrochemical reduction. This sensor showed a great sensitivity of 28.452 μA μM^{-1} cm^{-2} over the two linear regions (0.01 − 6 μM and 6 − 80 μM) of DA, with a low detection limit of 3.6 nM, stability of 2 weeks and satisfactory selectivity over common amino acids, UA, and AA. This improved performance of the sensor was accredited to its enhanced electro-active surface area and lowered the electron transfer resistant towards DA oxidation. But this sensor was validated for recognition of DA in human serum samples with decent recoveries (97.3–104.8%). ***Firooz et al.*** [61] demonstrated the Cu doped single phased,

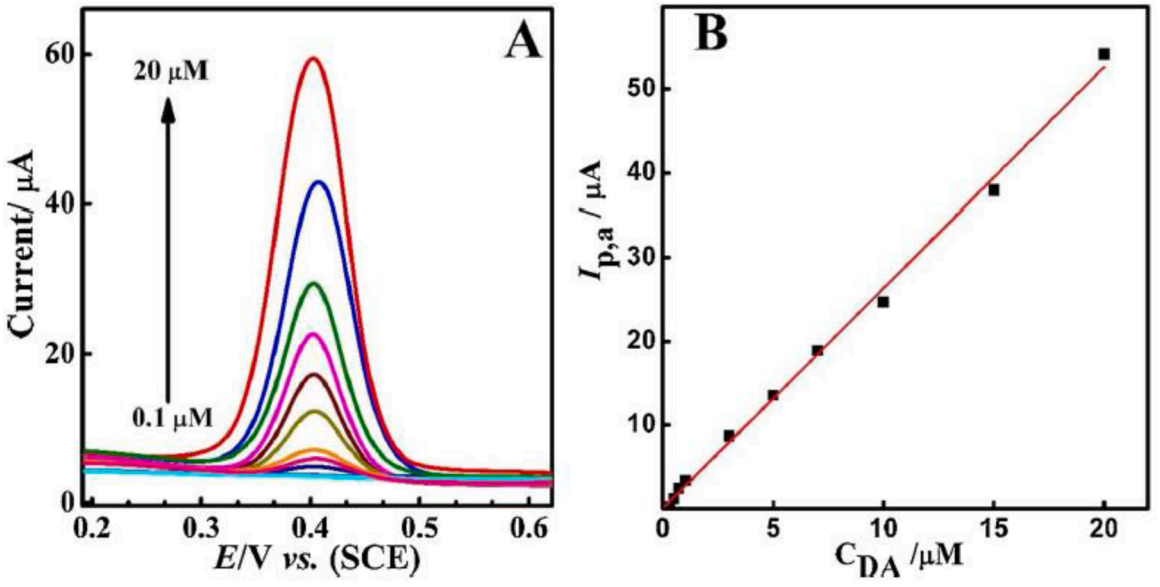

Fig. 2. DPVs of the 50% Cu doped ZnO based sensor for different concentrations of DA in the range of 0.1–20 μM in 0.04 M BR solution (pH 2.0), (B) The linear calibration plot of the the peak current vs. DA concentration, for the 50% Cu doped ZnO based sensor. Republished with permission from [61].

hexagonally ZnO plates for DA sensing where the composite was synthesized by the hydrothermal route. The electrode modified with the 50% Cu doped ZnO displayed the most encouraging performance with extraordinary stability over a wide range of pH values (2–8 pH). Fig. 2. **(A)** depicts the differential pulse voltammograms (DPVs) of the 50% Cu doped ZnO based sensor for different concentrations of DA in the range of 0.1–20 μM where the peak current increases with increasing concentration of DA because of the electro-oxidation of DA at this electrode surface. Fig. 2. **(B)** portrays corresponding calibration plot for various concentrations of DA. The sensor was able to detect low concentration of DA of 55 nM with a high sensitivity of 2630 nA μM^{-1}. This good performance of the sensor was due to high electrochemical active surface area of the electrode, an enhanced diffusion process of DA molecules at the electrode surface where the redox reaction occurred and greater catalytic activity resulting from the formation of droxyl functional groups on the electrode surface. But this sensor was not validated for practical applications. ***Gu et al.*** [62] presented the gold (Au) NPs functionalized ZnO-rGO composite based portable DA sensor where the composite was synthesized by wet-chemical route followed by electrodeposition. This sensor showed a wide linear range of 0.5 μM-100 μM and a low detection limit of 0.294 μM with decent stability and reproducibility.

2.1.4. Recognition of UA

Sensing of UA levels is essential in medical diagnostics as it is a vital biomarker and the ultimate product of purine metabolism in the human body. Insufficient supply of UA causes symptoms of diabetes mellitus, multiple sclerosis while greater levels of UA result in diseases like obesity, gout, arthritis, heavy hepatitis, neurological, cardiac and renal diseases. Recognition of UA can be realized by using uricase enzyme as a recognition element [63–64]. ***Liu et al.*** [65] developed single ZnO nanowire-based field effect transistors (FET) for enzymatic sensing of UA as displayed in Fig. 3. **(a)** where Fig. 3. **(b)** illustrates the optical image of it. The electrodes were passivated by polymethyl methacrylate (PMMA) to minimize the leakage current and eradicate the influence of metal–nanowire contact region thus confirming that the entire conductance changes originated from the nanowire only. Fig. 3. **(c)** exhibits the drain current (I_{ds}) vs. drain voltage (V_{ds}) characteristics of this biosensor acquired as a function of several gate voltages (V_g), signifying that the gate effect was a sign of an n-type semiconductor. The on/off ratio and transconductance were found to be ~4.6×10^6 and ~8.2 ns respectively. This biosensor was able to detect UA of as low as 1 pM over the region of 1 pM - 0.5 mM. But this sensor was validated for recognition of UA in real environs. ***Ali et al.*** [66] presented the ZnO quantum dots based UA electrochemical biosensor wherein the ZnO quantum dots with an average size of 4–6 nm were prepared by the precipitation technique. This three electrode based electrochemical biosensor was effectively fabricated on a flexible substrate, polyimide via screen printing method. Uricase immobilized this ZnO based sensor exhibited a good sensitivity of 4 $\mu A\ mM^{-1}\ cm^{-2}$ over the linear region of 1-10 mM with detection limit of 22.97 μM with good reproducibility. ZnO quantum dots amplified the surface area for the immobilization of uricase and sustained its bioactivity too. This sensor was also validated for recognition of UA in human urine samples with decent recoveries (96–104%). ***Ramya et al.*** [67] reported the ZnO nanoparticles based non-enzymatic UA sensor where the ZnO nanoparticles were prepared by crude black pepper seed extract as a stabilizing, capping, and bio-reducing agent, using inexpensive microwave irradiation method, optimized with three microwave irradiation times (5, 10, and 15 min). The ZnO NPs achieve from irradiation for 10 min showed the best crystallinity with flake-shaped morphology and an average size of 30 nm which subsequently used for successful UA sensing via electro-oxidation. In the course of catalytic oxidation of UA, Zn (II) was electrochemically oxidized to Zn (III), that was represented as an electron delivery system. This sensor revealed a good sensitivity of 40.485 $\mu A\ mM^{-1}\ cm^{-2}$ over the linear region of 50–500 μM of UA, with a low detection limit of 1.65 μM, stability of 24 days and reproducibility. This excellent performance was due to an increase in electron transfer rate originating from the enhanced crystallinity, and non-aggregated flake shaped with sharp-edged morphology of ZnO, mono dispersibility along with its high surface area. But selectivity of this sensor was not checked. This improved performance of the sensor was accredited to its enhanced electro-active surface area and lowered the electron transfer resistant towards UA oxidation. But this sensor was validated for recognition of UA in real environs. ***Alam et al.*** [68] described the doped ZnO-Ag_2O--Co_3O_4 nanoparticles based UA sensor where the composite was prepared by the co-precipitation technique. This sensor showed a high sensitivity of 82.3323 $\mu A\ \mu M^{-1}\ cm^{-2}$ over the linear region of 0.1 nM–0.01 mM of UA, with a very low detection limit of 89.14±4.46 pM, a decent response time of 22 s, stability of 7 days, selectivity and reproducibility. The practicality of this sensor was tested through for determination of UA in mouse serum, urine samples, and rabbit serum samples with satisfactory recovery% of ~100-123%. ***Veerla et al.*** [69] demonstrated the photo-responsive UA sensor by straight writing of ZnO pencil on paper using

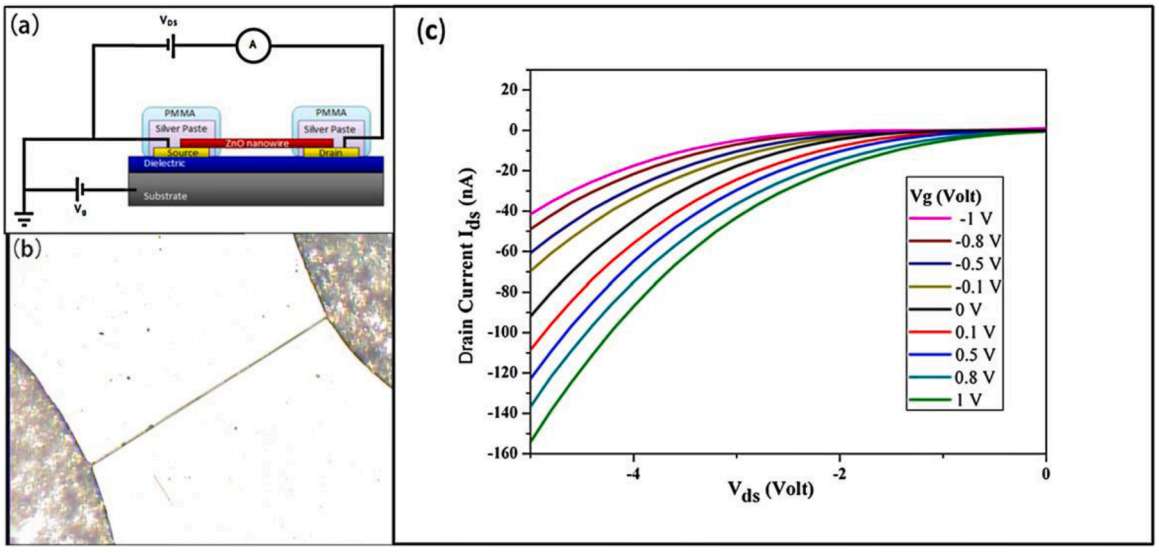

Fig. 3. (a) Diagram of single ZnO nanowire based FET biosensor, (b) optical image of biosensor and (c) I_{ds}–V_{ds} characteristics under varying V_g,Vds = −1 V. Reproduced with permission from [65].

the brilliant UV sensing feature of ZnO. This sensor displayed a good sensitivity of 1.99 μM^{-1} and LoD of 38.4 μM over the range of 100-450 μM of UA. In the presence of UA, the photogenerated electrons from ZnO under UV illumination get trapped by oxygen present in UA because of its oxidation in atmospheric air. With the increasing concentrations of UA, the oxidation of UA resulted in more photo-generated electron traps, thus leading towards further reduction in the photocurrent. ***Eryiğit et al.*** [70] reported the electrochemically rGO/zinc oxide (ErGO-ZnO) composite based UA sensor where this composite was synthesized by one-step electro-deposition method. This sensor exhibited a high sensitivity, low detection limit, good selectivity over AA, glucose, and other metal ions with decent repeatability, and stability of 20 days. A high analytical performance of this sensor was attributed to enhanced conductivity, enormous specific surface area of the composite. It was also able to sense UA in serum samples with recovery% of 97.4-103.2%. ***Samoson et al.*** [71] demonstrated the flexible laser induced Au NPs-chitosan-porous graphene based sensor for uric acid detection. This sensor showed a low the limit of detection of 0.33 μM over two linear ranges of 1–30 μM and 30–100 μM with a high sensitivity, good reproducibility and specificity. This composite based sensor unveiled an enhanced electrical conductivity and electrocatalytic activity toward the oxidation of UA. This sensor was validated through detection of UA in blood serum with recoveries between 86.6 ± 0.6 and 94.7 ± 0.4%.

2.1.5. Recognition of H_2O_2

Detecting H_2O_2 levels is indispensible as it is widely used as a crucial intermediary in food, environmental, and pharmacological industries. Overproduction of H_2O_2 results in the development of numerous diseases including cancer, diabetes, Parkinson's, Alzheimer's, and alcoholic liver disease. Recognition of H_2O_2 can be realized by using horseradish peroxidase enzyme as a recognition element [72]. ***Khan et al.*** [73] developed the Co doped ZnO nanoparticles based non-enzymatic H_2O_2 sensor where this composite was synthesized by a thermal technique. This sensor was able to determine H_2O_2 as low as 14.3 μM via its electro-catalytic reduction over the range of 5 – 30 mM with a sensitivity of 92.4444 μA mM^{-1} cm^{-2}. But the applicability, stability, reproducibility and selectivity of the sensor were not checked. ***Ke et al.*** [74] presented the Pt-ZnO nanotubes modified sensor for the recognition of H_2O_2 where the tubular structure of Pt-ZnO composite and the homogeneous distribution of Pt nanoparticles were prepared by one-pot electro-spinning of bipolymer, polyacrylonitrile and polyvinyl pyrrolidone in the presence of zinc acetate and chloroplatinic acid, followed by the calcination of nanofibers. An optimization study was done on the Pt/Zn molar ratio, to check its catalytic activity towards H_2O_2 reduction. The composite electrode with the Pt/Zn ratio of 1:3 showed the best catalytic performance, towards H_2O_2 sensing over the linear range of 20 μM – 5 mM with LoD of 1.5 μM and a sensitivity of 3.94 μA mM^{-1} and good selectivity over glucose, AA, UA and nitrite. This excellent performance was conceivably because of high electrical conductivity, enhanced electron transfer and great specific surface area of the Pt-ZnO nanotubes. But the applicability, stability, and reproducibility of the sensor were not checked. ***Rashed et al.*** [75] reported the mesoporous carbon doped ZnO composite based non-enzymatic H_2O_2 sensor where this composite was prepared by a F127 structural template agent in a modified sol-gel process followed by an ultra-sonication method. This sensor exhibited a high sensitivity of 0.04648 μA μM^{-1} cm^{-2} with low detection limit of 6.25 μM over the linear range of detection of 50 - 981 μM H_2O_2, good reproducibility, storage stability of 10 days, selectivity over nitrite, glucose etc. This enhanced performance of the sensor was attributed to (a) presence of more active site for ease in diffusion of H_2O_2 molecules resulting from its porous nature with smaller grain size, (b) huge specific sureface area originating from its nanostructure without any agglomeration, and (c) good electrical conductivity due to reduction in band gap from 3.19 (pristine ZnO) to 2.72 eV (composite). Besides, the fabricated sensor was validated through determination of H_2O_2 in tap water and milk samples with satisfactory recovery% of ~ 94.95 - 96.21%. ***Wu et al.*** [76] described the scavenger-free and self-powered photocathodic sensing system for H_2O_2 detection using the CuO-ZnO nanostructure. This photo-electrochemical sensor showed a sensitivity of 34.3 μA mM^{-1} cm^{-2} and 3.4 μA mM^{-1} cm^{-2} over two linear regions of H_2O_2 (0.2–1 mM and 1-8 mM) respectively with LoD of 8 μM. The CuO-ZnO photocathode revealed 2 folds greater photocurrent density than the pure CuO under simulated sunlight irradiation, accredited to the formation of CuO-ZnO heterojunction with well-aligned energy levels, thus offering excellent interfacial charge separation of photogenerated electron-hole pairs. Moreover, vertically aligned ZnO nanorods offered an enlarged surface area and close contact with CuO nanocrystals. But the applicability, stability, reproducibility and selectivity of the sensor were not tested.

2.1.6. Recognition of proteins and other biomarkers

Timely recognition of proteins and other biomarkers in human blood, urine, plasma and so on shows a dominant role in making proper therapeutic assessments for the management of diseases. Immunosensor, one kind of biosensors, has widely been used to detect biomolecules based on antigen (Ag) - antibody (Ab) interaction with good sensitivity and chiefly, excellent specificity [34]. ***Haque et al.*** [77] demonstrated the Cu doped ZnO nanoparticles based sensor for the determination of cardiac biomarker, myoglobin wherein this composite was prepared by the sol gel technique. An optimization was done to check the impact of Cu doping (13×10^{17}, 20×10^{17}, and 32×10^{17} atoms cm^{-3}) in the composite on sensing. The Cu (13×10^{17} atoms cm^{-3}) doped ZnO nanoparticles based sensor showed a great sensitivity of 10.14 μA nM^{-1} cm^{-2} with low detection limit of 0.46 nM over the linear range of detection of 3 - 15 nM myoglobin, good selectivity over cytochrome c, glucose etc. This boosted performance of the sensor was ascribed to direct electron transfer, and good electrical conductivity because of reduction in band gap from 3.91 (pure ZnO) to 3.6 eV (optimal composite). But reproducibility, storage stability and its validation were not assessed. ***Haque et al.*** [78] developed the Mn doped ZnO nanoparticles based sensor for the sensing of myoglobin wherein this composite was prepared by the sol-gel method. An optimization was accomplished to observe the influence of Mn doping (13×10^{17}, 20×10^{17}, and 32×10^{17} atoms cm^{-3}) in the composite on sensing. The Mn (13×10^{17} atoms cm^{-3}) doped ZnO nanoparticles based sensor revealed a high sensitivity of 95 μA nM^{-1} cm^{-2} with low detection limit of 0.35 nM over the linear range of detection of 3 - 15 nM myoglobin, decent selectivity over cytochrome c, HSA. This good performance of the sensor was attributed to direct electron transfer, and enhanced electrical conductivity owing to decrease in the band gap from 3.59 (pure ZnO) to 1.95 eV (optimal composite). But reproducibility, storage stability and its validation were not evaluated. ***Ibupoto et al.*** [79] presented the disposable potentiometric antibody immobilized ZnO nanotubes based sensor for the sensing of C-reactive protein (CRP)-Ag, a cytokine-induced "acute phase" protein wherein the monoclonal anti-CRP clone CRP-8 (mouse lgG1 isotype) with glutaraldehyde was immobilized on the surface of this biosensor using physical adsorption technique. The Ab immobilized biosensor was able to sense the CRP over the range 1×10^{-5} mg/L - 10 mg/L with a satisfactory sensitivity of 13.17± 0.42 mV/decade, LoD of 1 μg/L, response time of 10 s, decent reproducibility, repeatability, selectivity over glucose, urea, UA, Na, K, Fe ions, and poor stability of 3 days. But its validation in real samples was not measured. ***Dong et al.*** [80] reported the ZnO-porous carbon composite for the immunosensing of CRP where the carbon-based composite was achieved through thermolysis of metal-organic framework. This composite and ionic liquid (IL) composite membrane based biosensor showed a low detection limit of 5 pg/mL over the region of 0.01–1000 ng/mL CRP with good selectivity over bovine serum albumin, immunoglobulin G, glucose, AA and UA, reproducibility and durability of 4 weeks. This good performance was due to high conductivity, controllable morphologies and biocompatibility of this composite

towards the recognition of CRP. The applicability of the biosensor was examined through recognition of CRP in human serum with the recovery % of 94.5-107%. ***Madhu et al.*** [81] described the ZnO nanorods incorporated flexible carbon fibers for immunosensing of sweat cortisol where the ZnO nanorods coated flexible carbon yarns were synthesized via the hydrothermal route for the immobilization of anti-cortisol Ab. This biosensor exhibited a low detection limit of 0.098 fg/mL over the concentration range of 1 fg/mL - 1 μg/mL with brilliant mechanical stability, superwettable properties, biocompatibility, good reproducibility, selectivity over progesterone, testosterone, corticosterone, cortisone, cholesterol, glucose, UA, urea etc., stability of 1 month. The feasibility of this immunosensor was checked through successful detection of cortisol in sweat with the recovery% of 96.77- 103.36%. ***Chakraborty et al.*** [82] demonstrated the ZnO thin film based FET biosensor for identifying PSA after anti-PSA Ab immobilization wherein the ZnO thin film was prepared by the electron beam evaporation by varying deposition time and current to adjust the surface roughness and defect state density. Although the transconductance of the FET biosensor degraded monotonically with the increasing defect density, the Ab binding density showed a non-monotonic behavior which was accredited to the increment of surface roughness further than a definite limit, thus, reducing the active area required for Ab capture. This optimal sensor showed a low detection limit of 0.06 fM with good reproducibility, selectivity and durability of 2 months. But its validation in real samples was not tested. ***Shabani et al.*** [83] developed the ZnO nanorods modified immunoassay for fast recognition of the matrix metalloproteinase9 (MMP-9) biomarker based on the immobilization of Ab. This biosensor showed a sensitivity of 32.5 μA/(decade × cm^2) over the linear range of 1–1000 ng/mL with a high detection time of 35 min, detection limit of 0.15 ng/mL. But its selectivity and storage stability were not checked. Furthermore, its validation in human serum samples was tested and results were also compared with the commercial enzyme-linked immunosorbent assay displaying less than 8% difference. ***Yang et al.*** [84] presented the free-standing ZnO nanosheets grown on 2D thin-layered MoS_2 based biosensor for detection of single-stranded DNA (ssDNA) wherein MoS_2 was synthesized by an ultrasonic exfoliation way from bulk MoS_2 followed by electrodeposition of the ZnO nanosheet on the MoS_2 scaffold. The partly negatively charged MoS_2 layer helped towards the nucleation and growth of ZnO nanosheets via the electrostatic interactions. And the results demonstrated that the free-standing ZnO-MoS_2 nanosheets had low detection limit (6.6 × 10−16 M) and has a positive influence on DNA immobilization and hybridization. This optimal bioelectrode was able to detect 6.6×10^{-16} M of ssDNA over the dynamic range of $1 \times 10^{-15} - 1 \times 10^{-6}$ M with good reproducibility and regeneration ability without losing its sensitivity. But its validation was not checked in real samples. ***Cao et al.*** [85] reported the piezotronic effect enhanced label-free DNA sensing with the schottky-contacted ZnO nanowire based FET biosensor where this device was functionalized with ssDNA. The ssDNA can selectively hybridize with the target complementary DNA (cDNA) as the negatively charged target cDNA is complementary to the ssDNA. As soon as the cDNA was hybridized with the ssDNA decorated on ZnO nanowire, it was adsorbed on the surface of the ZnO nanowire, thus performing the sensing of cDNA. Piezotronic influence on the performance of this biosensor was studied by assessing its output current under various compressive strains and target cDNA concentrations over the range of $1 \times 10^{-10} - 1 \times 10^{-7}$ M with good selectivity over non-complementary DNA. But its longevity and applicability were not evaluated. ***Murugan et al.*** [86] described the three layered ZnS-ZnO-Ta_2O_5 (core) − SiO_2 (shell) nanoparticles based enzymatic sensor for the recognition of non-neurally secreted cancer biomarker, acetylcholine where this composite was synthesized in two steps using the solvothermal method. Acetylcholinesterase was used as an enzyme. An optimization study was carried out by varying the compositions of ZnS, ZnO, Ta_2O_5, and SiO_2 in their layers to observe impact of each constituent on sensing. The composite synthesized at 0.15 wt % $ZnCl_2$ concentration showed a very low limit of detection of 0.0116 μM over the concentrations range of 0.1-1200 μM of acetylcholine with decent repeatability and reproducibility. This good performance was due to high specific surface area of 1091 m^2/g and high conductivity of the optimal composite. The practicality of this sensor was validated through determination of acetylcholine in blood serum samples with an acceptable recovery range of 99−101.3%.

2.2. Environmental monitoring applications

Recently, with the fast economic development, ecological pollution is becoming more severe. Enormous amounts of trashes and toxic chemicals used in normal life, industry and cultivation, are discharged into the environments. An excessive number of these chemicals are perilous, cancer-causing and straightforwardly come into the food chain, which have endangered rigorously the environments along with the social health. Therefore, it is noteworthy to fabricate sensitive, inexpensive sensors for checking and recognition of the priority pollutants including heavy metal ions, phenolic compounds, hydrazine and other organic molecules.

2.2.1. Recognition of phenolic compounds

One of the most common pollutants is phenol, and its derivatives which are commonly available in industrial waste, food, plastic, pharmaceutical industries. It causes various fatal diseases like muscular retardation fits, paroxysm, respiratory effects, cancer, and so on. 1 g of phenolic compounds can even cause the death of human beings. According to the Bureau of Indian Standards (BIS), the maximum permissible limit of phenol in water bodies is 1 mg L^{-1}. Among all the nanosensors, ZnO-based sensors are extensively testified for detection of phenol, offering excellent sensitivity and lower detection limits. ***Sha et al.*** [87] demonstrated a novel non-enzymatic method for the sensing of phenol using rGO - ZnO composite wherein the composite was prepared by an in-situ wet chemical method from the precursors, GO and Zinc acetate. The electrode surface was modified by the composite which successfully eliminated the surface fouling effect through the precise selection of the sensing peaks. This sensor exhibited a good sensitivity, low detection limit of 1.94 μM with good linearity, reproducibility, selectivity and stability. ***Balkhoyor et al.*** [88] developed the Ce-doped ZnO nanostructures based phenol sensor wherein the composite was synthesized by a simple wet chemical technique with the help alkali medium as a reducing agent. This sensor showed a brilliant sensitivity of ∼ 94.937 μA μM^{-1} cm^{-2} with good reproducibility, long-term stability and high selectivity towards phenol detection. The excellent performance was due to the enhanced oxygen absorption ability of the active material thus, assisting in rapid oxidation of phenol. The composite modified sensor is displayed in Fig. 4. **(a),** while Fig. 4. **(b)** depicts the calibration plot over the concentration range of phenol from 0.9 nM - 0.9 mM. The comparative I-V responses of the sensors towards phenol are presented in Fig. 4. **(c)**, whereas the sensing mechanism of phenol is displayed in Fig. 4. **(d).**

Arfin et al. [89] presented the ZnO functionalized GO composite based phenol sensor. This sensor displayed a very low detection limit of 2.2 nM with excellent selectivity, stability of 30 days and reversibility over the range of 5–155 μM of phenol. ***Rahman et al.*** [90] reported the germanium-doped ZnO composite for 4-aminophenol sensing. This sensor showed a sensitivity of be 0.5063 μA μM^{-1} cm^{-2} with detection limit of 0.5925 ± 0.02 nM. This good sensing performance was attributed to fast and high oxidizing capability of this electrode. This senor was validated through detection of 4-aminophenol in real samples like industrial waste water and tap water with good recovery%. ***Wahid et al.*** [91] described the Nd_2O_3-ZnO composite based sensor used for detection of toxic 2,4-Dinitrophenol wherein this composite was prepared by one-pot wet chemical technique. This sensor exhibited an excellent sensitivity of 28.481 nA nM^{-1} cm^{-2} with low detection limit of 0.33 pM.

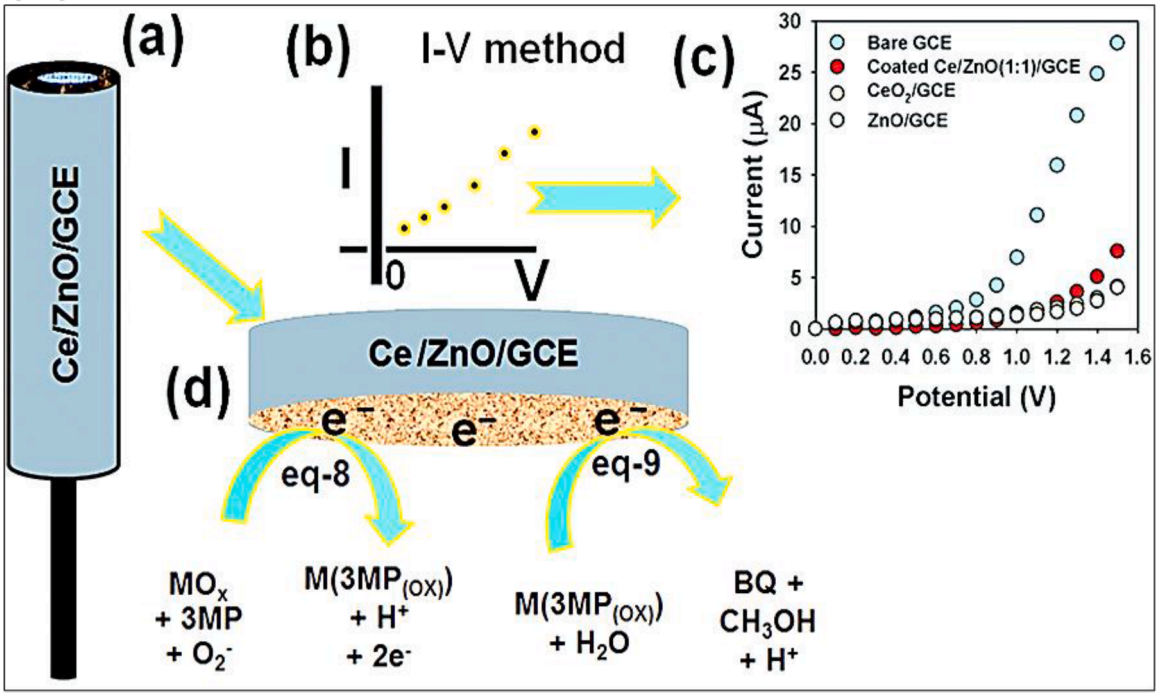

Fig. 4. (a) Diagram of the composite modified sensor; (b) the calibration plot over the concentration range of phenol from 0.9 nM - 0.9 mM, (c) The comparative I-V responses of the sensors towards phenol; (d) The sensing mechanism of phenol at the surface Ce-dopped ZnO; Reproduced with permission from [88].

2.2.2. Recognition of Hydrazine

Hydrazine is considered as a neurotoxic material. It has carcinogenic and mutagenic effects. It can cause severe damage to the liver, lungs, kidneys, and human central nervous system. Moreover, it is expansively used in several industrial applications as catalysts, emulsifiers, antioxidants etc. Hence, an accurate recognition of hydrazine is of prime significance. ***Ahmad et al.*** [92] demonstrated the vertically aligned ZnO nanorods based hydrazine sensor wherein the nanorods were grown on the Ag electrode via a wet chemical technique. Hydrazine was detected via its oxidation at the surface of the ZnO nanorods modified electrode as displayed in **Fig. 5.** This sensor showed a sensitivity of 105.5 μA μM^{-1} cm^{-2}, with low detection limit of 0.005 μM and a long term stability of

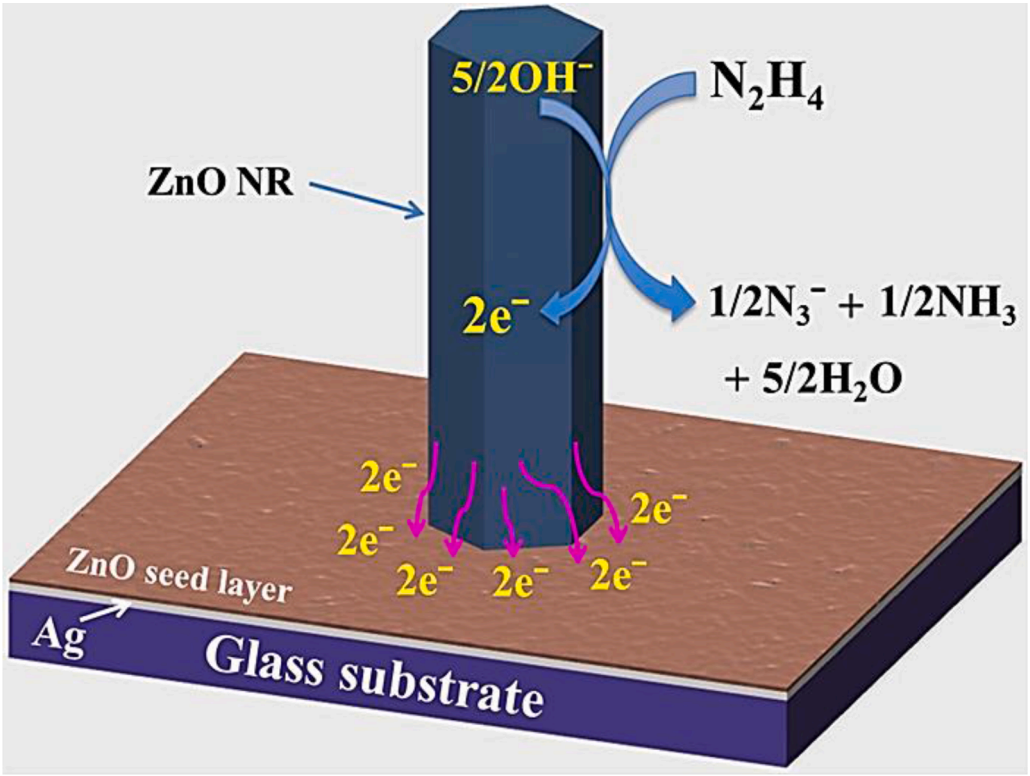

Fig. 5. The sensing mechanism of phenol at the surface of ZnO nanorods based electrode; Reproduced with permission from [92].

60 days.

Rahman et al. [93] developed the Sn doped ZnO nanoparticles modified hydrazine sensor. This senor showed a sensitivity of 5.0108 μA μM^{-1} cm^{-2} with a detection limit of 18.95 ± 0.02 pM ad good linearity over the contration range of 2 nM - 20 mM of hydrazine. Higher sensitivity of the electrode was ascribed to its high electron transfer rate capability. ***Ismail et al.*** [94] presented the mesoporous Au-ZnO nano-composite based hydrazine sensor where the composite was prepared via the photochemical reduction technique. The use of Au in ZnO enhances the ability of oxidation towards hydrazine determination. The stability of the device was poor as compared to the literature. Its performance was decreased to 5% just after 45 minutes of operation. ***Umar et al.*** [95] reported the ZnO nanowires based amperometric hydrazine sensors where the ZnO nanowires showed a high aspect ratio with urchin-like morphologies. This sensor exhibited a sensitivity of 12.76 μA nM^{-1} cm^{-2} with low detection limit of 84.7 nM, fast response time (<5 s) and good stability of 35 days over the linear range of 500 -1200 nM. This excellent sensing performance was due to its high specific surface area resulting from nano-wired structure with high aspect ratio. ***Mehta et al.*** [96] described the well crystallized ZnO nanoparticles based ultra-sensitive hydrazine sensor whereas the nanoparticles were prepared by the wet chemical method at 90 ℃. This sensor revealed a good sensitivity of ~97.133 μA μM^{-1} cm^{-2} with low-detection limit of 147.54 nM. ***Kumar et al.*** [97] demonstrated the ZnO nanocones based hydrazine sensors. This sensor exhibited a high sensitivity of 50×10^4 μA μM^{-1} cm^{-2} with a detection limit of 0.01 μM with quick response time of < 2 s. ***Jang et al.*** [98] reported the poly (vinylidene fluoride-co-hexafluoropropylene) (PVDF-HFP) functionalized ZnO thin-film transistor (TFT)-based water-stable hydrazine sensor. This sensor displayed an excellent repeatability and stability to DI water and hydrazine, thus signifying its high sensitivity, low detection limit of 0.01 nM with acceptable reproducibility. This exceptional sensing performance was accredited to the improved surface interaction between PVDF-HFP with a strong dipole moment and hydrazine, which was completely differentiated from the conventional sensing mechanism associated with oxygen ion species in ZnO. ***Mousavi-Majd et al.*** [99] described the zeolitic imidazolate framework derived porous ZnO-Co_3O_4 incorporated with Au NPs as ternary composite for sensing of hydrazine in alkaline media. This sensor exhibited a wide dynamic range, high sensitivity, and acceptable specificity with extraordinarily lower oxidation potential and limit of detection as compared to only ZnO--Co_3O_4 composite. These excellent performances were attributable to the porous structure of ZnO-Co_3O_4, great conductivity of Au NPs, and the synergic effect among the elements. ***Ibrahim et al.*** [100] developed the Ag-doped ZnO nanoflower based sensor for sensing of phenyl hydrazine wherein the nanostructure was synthesized by a hydrothermal technique. This sensor exhibited a sensitivity of ~557.108 ± 0.012 mA (mol L^{-1})$^{-1}$ cm^{-2} with a low detection limit of ~5 × 10^{-9} mol L^{-1} and the response time of 10 s. Though the detection limit was low, the sensitivity was very less as compared with the available literature. ***Umar et al.*** [101] presented the In-doped ZnO nanorods and nanodisks based sensors for recognition of phenyl hydrazine wherein the In-doped ZnO was prepared by thermal evaporation route from the precursors, metallic zinc and indium powders in the presence of oxygen. The nanorods and nanodisks based sensors exhibited a sensitivity of 70.43 μA•mM^{-1} cm^{-2} and 130.18 μA•mM^{-1} cm^{-2} respectively with a detection limit was 0.5 μM, over the linear range of 0.5 μM – 5 mM.

2.2.3. Recognition of explosives

The ecological contamination activated by lethal, inorganic or organic molecules like explosives and pharmaceuticals have attracted wide attention among research communities because of their negating effects in humans. These molecules are recognized by either oxidation or reduction at the electrode surface. Determination of other pollutants like nitro based compounds and nitro-substituted aromatic explosives like 2,4,6-trinitrotoluene (TNT), dinitrotoluene (DNT), 4-nitrotoluene (4-NT), picric acid and hexogen (RDX), etc. are significant due to their harmful effects [34]. ***Ibrahim et al.*** [102] reported the ZnO nano-peanuts based sensor for the detection of picric acid where the active material was prepared by a hydrothermal method. This sensor revealed a sensitivity of 493.64 μA mM^{-1} cm^{-2} with a detection limit of 0.125 mM over a linear dynamic range of 1 – 5 mM. The detection limit was very poor as compared to the literature. Moreover, reproducibility, stability etc. other important characteristics of a sensor were not investigated. ***Mohammad et al.*** [103] described the ZnO - graphitic carbon nitride (g-CN) nanohybrid based sensor for the recognition of 4-NT and DNT wherein this nano-hybrid was prepared by an in-situ one pot solid-state thermal decomposition technique. The sensor displayed good electrochemical performance in terms of detection limit, sensitivity, selectivity, repeatability, reproducibility and stability of 2 weeks. The attractive performance of the ZnO-g-CN nanohybrid towards the recognizing of -NO_2 containing aromatics was attributed to its high surface area, enhanced electrical conductivity and the formation of hetero-junction between the interfaces of ZnO and g-CN. ***Yang et al.*** [104] demonstrated the ZnO-MoS_2 composite based TNT sensor wherein vertically oriented ZnO nanosheets were electro-deposited on the surface of the MoS_2 based electrode. This sensor showed a sensitivity of 1.55 μA ppm^{-1} with a detection limit of 5.2×10^{-5} ppm, good reproducibility over the range of 1×10^{-4} -1 ppm of TNT. The nitro group of TNT was electro-reduced through a two-electron transfer method, thus helping the reduction of hydroxylamine group into an aromatic amine. ***Wang et al.*** [105] developed the N-rich C@graphitic carbon-coated ZnO nanowire arrays on a graphene fiber (ZnO@C/GF) based sensor for the sensing of TNT. This sensor showed good sensitivity, selectivity and stability of 2 weeks. The sensor was validated through detection of TNT in lake water and tap water with acceptable recovery %.

2.2.4. Recognition of heavy metal ions

Detecting of toxic heavy metal ions like copper (Cu^{2+}), lead (Pb^{2+}), cadmium (Cd^{2+}), mercury (Hg^{2+}), chromium (Cr^{3+}), and so on in water bodies is of major importance because of their quick accumulation, harmfulness in the human body, and non-biodegradability. ***Kim et al.*** [106] presented the ZnO nanoglobules-GO and ZnO nanoglobules-rGO based multiple ion (MI) FET sensors for Cr^{3+} and Cu^{2+} sensing respectively. These sensors showed excellent sensing performances in terms of good sensitivity, stability, selectivity and low detection limit which were accredited to improved heterogeneous electron transfer process, well dispersed morphology of the composites and large number of active sites. ***Oliveira et al.*** [107] reported the sensor using ZnO nanofibers functionalized by L-cysteine for recognition of Pb^{2+} ions. ZnO nanofibers were synthesized via electro-spinning technique and L-cysteine was affixed on the surface of ZnO nanofibers. This sensor showed brilliant sensitivity, selectivity, and stability of 20 days with a limit of detection of 0.397 μg L^{-1} over the linear range of 10–140 μg L^{-1}. The sensor was effectively employed for sensing of Pb^{2+} ions in lake water and tap water samples with good recovery %. Its good performance was due to presence of high porosity of nanofibers along with Lewis acid-base interaction of L-cysteine. ***Moutcine et al.*** [108] described the a phosphate-ZnO based electrode for concurrent recognition of Cd^{2+} and Hg^{2+} via electro-oxidation as depicted in **Fig. 6** where the ZnO nanoparticles was prepared via the doping of natural phosphate with Zn. It showed a low detection limit, high sensitivity and good linearity. This sensor was also utilized to check successfully the concentrations of Cd^{2+} and Hg^{2+} in drinking water with decent recovery% (95-97.5%). ***Karthik et al.*** [109] demonstrated the Co doped ZnO-rGO nanorods based sensor for the recognition of Cd^{2+} and Pb^{2+} via electro-oxidation where the composite was prepared through the chemical co-precipitation technique. This sensor exhibited good sensitivity, low detection limit, satisfactory selectivity, and reproducibility. Its applicability in real environs was effectively assessed by sensing ions in tap water with good recovery% (99.06% - 101.33%). ***Kim et al.*** [110] developed the ZnO-GO and ZnO-rGO based FET sensors for trace level recognition of Cr^{3+} and

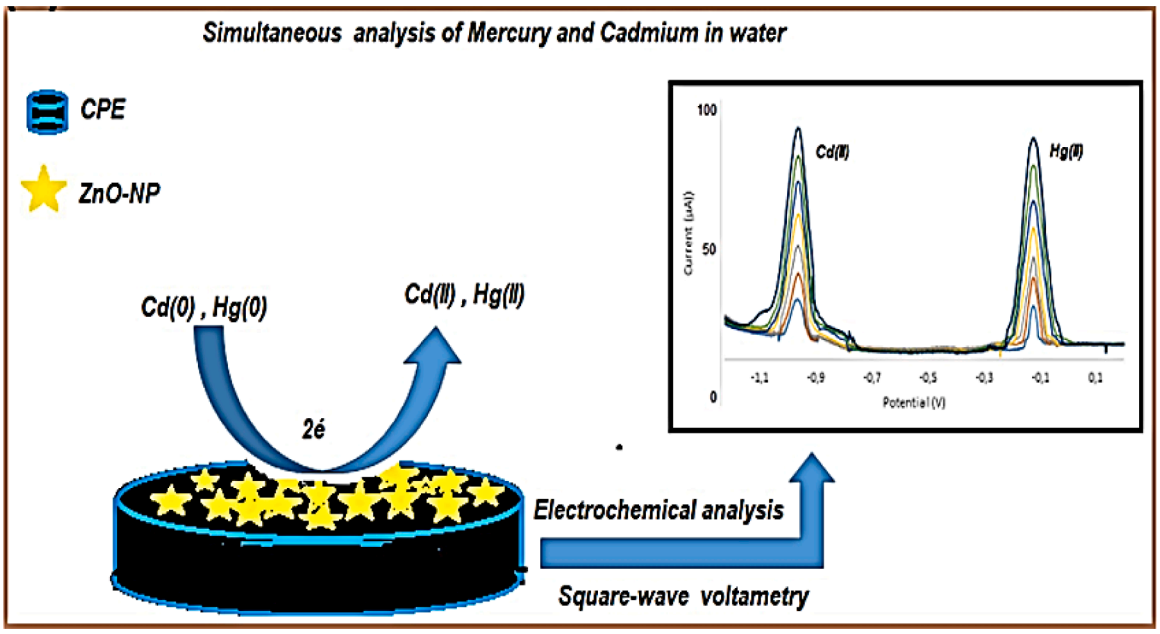

Fig. 6. The sensing mechanism of Cd^{2+} and Hg^{2+} via electro-oxidation at the surface of phosphate-ZnO based electrode; Reproduced with permission from [108].

Cu^{2+} ions. These sensors revealed the notable sensitivities, good dynamic linear range of heavy metal ions with low detection limit of ~7.05 μM and ~14.9 μM ZnO-GO and ZnO-rGO based FET sensors, respectively. Effective charge transfer over electrode significantly improved the trace detection of Cr^{3+} and Cu^{2+} ions. Theses fabricated FET based sensing platforms also unveiled an excellent reproducibility and stability, therefore, confirming enormous prospective to develop a beneficial tool for water conserving system. A summary of the reported ZnO nano-structured based devices in chemical sensing applications was summarized in **Table 1**.

3. Applications of ZnO nano-structured based devices for optical sensing

Rapid development in the field of metal-organic halide perovskite and the dye-sensitized solar cell (DSSC) is motivating the research community to explore different metal oxides to be used in these devices. ZnO is one of the emerging inorganic semiconductor materials due to its easy synthesis, direct electron pathways, low cost of fabrication and large variety of nanostructures. In this part of the review article, the main focus is on the recent developments of ZnO nano-structures in the application of perovskite and dye-sensitized solar cell. The recent state-of-art scenario of the ZnO based PSCs and DSSCs are mainly discussed along with some other application of ZnO nanostructures as an optical sensor. Recent challenges and future scope of ZnO nanostructure in the field of optical sensor is also discussed.

3.1. In perovskite solar cells (PSCs)

PSCs are mainly photo-electrochemical devices, having a mesoporous metal oxide film with a layer of perovskite sensitized material, a metal electrode and a hole transport layer. The oxide layer plays a crucial role as the carrier mobility of this layer is very important to achieve high photovoltaic performance [111]. A number of stable metal oxides like TiO_2 [112], ZnO [113], SnO_2 [114] can be used in PSCs. TiO_2 is a very promising metal oxide to be used in perovskite solar cell as an electron transport layer (ETL) but due to its fabrication complexity, like post deposition treatment at high annealing temperature, the possibility of using this layer in flexible PSCs are hindered. Due to this, there is a massive search of other metal oxide semiconductor which allows low temperature processing also. ZnO is a suitable material and can be an alternative of TiO_2 to be used in PSCs as it has high energy band gap and physical properties similar to TiO_2 material. Moreover ZnO can be deposited by several low temperature deposition processes to get structures with different morphology. Also the properties of ZnO can easily be tuned by modifying the morphology, doping and structural parameters [115]. Recent studies show that the use of ZnO layer in the PSCs is beneficial in terms of their enhanced efficiency due to its excellent electrical characteristics also [116]. ***Xiong et al.*** [117] reported the structure of growth process of ZnO nanorods by hydrothermal method. The ZnO crystals, growing along the C axis are responsible for the generation of nanorods. The nanorods were of 0.84 μm in length and 0.14 μm in diameter. The nanorods were in hexagonal structure with preferred orientation along (100). **Fig. 7.** shows the typical device structure with carrier transport mechanism for ZnO nanostructure based perovskite solar cells.

To develop PSCs having high efficiency and cost-effective, two different schemes are adopted by the research community. Firstly, to use a nano-structure oxide layer which can work as an ETL and another is to develop a planer heterojunction or planer structure. In the first model, TiO_2 films are used but this films need to be processed at a very high annealing temperature. So instead of using TiO_2, the research community is now looking after ZnO films which can also be used as an ETL in PSCs. In the year of 2014, ***Son et al.*** [118] reported the ZnO nanorod based PSCs. In this work, ZnO nanorods were grown on ZnO seed layer using chemical processes. The dimensions of the nanorods like the diameter and the lengths were controlled by the solution concentration and deposition time. The reported solar cell exhibits an efficiency of 11.13% with a V_{oc} of 0.99 V, J_{sc} of 20.08 mA.cm^{-2} and FF of 0.56. Also the external quantum efficiency (EQE) was almost above 80% for the wavelength range of 400 to 750 nm. It is also found from the photocurrent response that the charge collection was rapidly saturated for ZnO based devices in comparision with TiO_2 based perovskite solar cells. So the ZnO nanorods are the effective means of charge collection for the PSCs. The state-of-art efficiency obtained from PSCs having ZnO mesophorous ETMs and ZnO planer heterojunction are 16.1% [119] and 18.9% [120] respectively. ***Mahmood et al.*** [119] presented the use of N_2 doped ZnO nanorods as electron transporting materials (ETMs) for the application in perovskite solar cells. N_2 doped ZnO NR arrays helping in a better way to shift the work function which leads to get a boost in the

Table 1
List of ZnO nano-structured based devices in chemical sensing applications.

Nanomaterial	Analytes	Approach	Sensitivity	Detection limit	Linear Range [Ref]
Co-Fe doped ZnO	Glucose	Enzymatic	32.2 μA mM^{-1} cm^{-2}	0.27 mM	0-4 mM [42]
ZnO-Pt-CS	Glucose	Enzymatic	62.14 μA mM^{-1} cm^{-2}	16.6 μM	100 μM-2 mM [43]
Pt nanodendrites - ZnO nanorods	Glucose	Enzymatic	98.34 μA mM^{-1} cm^{-2}	30 μM	0.05–1 mM [44]
Cu-ZnO nano-thorn	Glucose	Non-enzymatic	63.76 μA mM^{-1} cm^{-2}	3.762 μM	0.1–4.5 mM [45]
Au-ZnO nanorods	Glucose	Non-enzymatic	4416 μA mM^{-1} cm^{-2}	0.12 μM	0.001–15 mM [46]
ZnO quantum dots –MWCNTs	Glucose	Non-enzymatic	9.36 μA μM^{-1}	0.208 μM	0.1 - 2.5 μM [47]
Pt- g-C_3N_4- ZnO	Glucose	Non-enzymatic	3.34 μA mM^{-1} cm^{-2}	0.1 μM	0.25–110 mM [48]
Cu_2O-ZnO	Glucose	Non-enzymatic	441.2 μA mM^{-1} cm^{-2}	0.13 μM	0.02–1 mM [49]
ZnO nanorods	Glucose	Non-enzymatic	91.8 μA mM^{-1} cm^{-2}	-	- [50]
mg-ZnO@$Ni(OH)_2$ NSs	Glucose	Non-enzymatic	259.78 and 62.82 μA mM^{-1} cm^{-2}	0.06 μM	0.084 – 0.941 mM and 0.941–6.50 mM [51]
Vertically aligned ZnO nanorods	Urea	Enzymatic	41.64 μA mM^{-1} cm^{-2}	10 μM	0.001–24 mM [53]
Nanoporous ZnO film	Urea	Enzymatic	0.0506 kΩ/(mg dL^{-1})	5 mg dL^{-1}	8.0–110.0 mg dL^{-1} [54]
ZnO-rGO	Urea	Non-enzymatic	682.8 μA mM^{-1} cm^{-2}	0.012 μM	0.02 - 7.2 μM [55]
Ag-ZnO nanorods	Urea	Non-enzymatic	-	-	- [56]
ZnO encapsulated polyaniline-grafted CS composite	Urea	Enzymatic	187.5 μV ppm^{-1} cm^{-2}	29.84 ppm	20 - 500 ppm [57]
Carbon-ZnO microfibers	DA	Non-enzymatic	-	0.106 μM	0 - 50 and 50 - 300 μM [59]
ZnO nanorods-rGO	DA	Non-enzymatic	28.452 μA μM^{-1} cm^{-2}	3.6 nM	0.01− 6 μM and 6 − 80 μM [60]
Cu doped ZnO	DA	Non-enzymatic	2630 nA μM^{-1}	55 nM	0.1–20 μM [61]
Au NPs functionalized ZnO-rGO	DA	Non-enzymatic	-	0.294 μM	0.5 - 100 μM [62]
ZnO based FET	UA	Enzymatic	-	1 pM	1 pM - 0.5 mM [65]
ZnO quantum dots	UA	Enzymatic	4 μA mM^{-1} cm^{-2}	22.97 μM	1-10 mM [66]
ZnO nanoparticles	UA	Non-enzymatic	40.485 μA mM^{-1} cm^{-2}	1.65 μM	50–500 μM [67]
ZnO-Ag_2O-Co_3O_4 nanoparticles	UA	Non-enzymatic	82.3323 μA μM^{-1} cm^{-2}	89.14±4.46 pM	0.1 nM–0.01 mM [68]
ZnO pencil	UA	Non-enzymatic	1.99 μM^{-1}	38.4 μM	100-450 μM [69]
ErGO-ZnO	UA	Non-enzymatic	150.7 μA mM^{-1} cm^{-2}	0.45 μM	1−400 μM [70]
Au NPs – chitosan - graphene	UA	Non-enzymatic	-	0.33 μM	1–30 μM and 30–100 μM [71]
Co doped ZnO nanoparticles	H_2O_2	Non-enzymatic	92.4444 μA mM^{-1} cm^{-2}	14.3 μM	5 – 30 mM [73]
Pt-ZnO nanotubes	H_2O_2	Non-enzymatic	3.94 μA mM^{-1}	1.5 μM	20 μM – 5 mM [74]
Mesoporous carbon doped ZnO	H_2O_2	Non-enzymatic	0.04648 μA μM^{-1} cm^{-2}	6.25 μM	50 - 981 μM [75]
Vertically aligned ZnO nanorods - CuO nanocrystals	H_2O_2	Non-enzymatic	34.3 μA mM^{-1} cm^{-2} and 3.4 μA mM^{-1} cm^{-2}	8 μM	0.2–1 mM and 1-8 mM [76]
Cu doped ZnO nanoparticles	Myoglobin	Non-enzymatic	10.14 μA nM^{-1} cm^{-2}	0.46 nM	3 - 15 nM [77]
Mn doped ZnO nanoparticles	Myoglobin	Non-enzymatic	95 μA nM^{-1} cm^{-2}	0.35 nM	3 - 15 nM [78]
ZnO nanotubes	CRP	Ag-Ab interaction	13.17± 0.42 mV/decade	1 μg/L	1 × 10^{-5} mg/L - 10 mg/L [79]
ZnO-porous carbon composite	CRP	Ag-Ab interaction	-	5 pg/mL	0.01–1000 ng/mL [80]
ZnO nanorods incorporated flexible carbon fibers	Cortisol	Ag-Ab interaction	-	0.098 fg/mL	1 fg/mL - 1 μg/mL [81]
ZnO thin film based FET	PSA	Ag-Ab interaction	-	0.06 fM	- [82]
ZnO nanorods	MMP-9	Ag-Ab interaction	32.5 μA/(decade x cm^2)	0.15 ng/mL	1–1000 ng/mL [83]
Free-standing ZnO nanosheets grown on MoS_2	ssDNA	Hybridization	-	6.6 × 10^{-16} M	1 × 10^{-15} – 1 × 10^{-6} M [84]
ZnO nanowire based FET	cDNA	Hybridization	-	-	1 × 10^{-10} – 1 × 10^{-7} M [85]
ZnS-ZnO-Ta_2O_5 (core) − SiO_2 (shell) nanoparticles	Acetylcholine	Enzymatic	-	0.0116 μM	0.1-1200 μM [86]
ZnO-rGO	Phenol	Non-enzymatic	1.79 μA μM^{-1} cm^{-2} 0.389 μM^{-1} cm^{-2}	1.94 μM	2 – 15 μM 15 – 40 μM [87]
Ce-doped ZnO nanostructure	Phenol	Non-enzymatic	~ 94.937 μA μM^{-1} cm^{-2}	11.5 ± 0.2 pM	0.9 nM - 0.9 mM [88]
ZnO-GO	Phenol	Non-enzymatic	-	2.2 nM	5 – 155 μM [89]
Germanium-doped ZnO	4-aminophenol	Non-enzymatic	0.5063 μA μM^{-1} cm^{-2}	0.5925 ± 0.02 nM	0.1 nM - 0.1 mM [90]
Nd_2O_3-ZnO	2,4-Dinitrophenol	Non-enzymatic	28.481 nA nM^{-1} cm^{-2}	0.33 pM	1 pM – 0.1 mM [91]
ZnO nanorods	Hydrazine	Non-enzymatic	105.5 μA μM^{-1} cm^{-2}	0.005 μM	0.01–98.6 μM [92]
Sn doped ZnO nanoparticles	Hydrazine	Non-enzymatic	5.0108 μA μM^{-1} cm^{-2}	18.95 ± 0.02 pM	2 nM - 20 mM [93]
Mesoporous Au-ZnO	Hydrazine	Non-enzymatic	0.873 μA μM^{-1} cm^{-2}	0.242 μM	0.2 – 14.2 μM [94]
ZnO nanowires	Hydrazine	Non-enzymatic	12.76 μA nM^{-1} cm^{-2}	84.7 nM	500 - 1200 nM [95]
ZnO nanoparticles	Hydrazine	Non-enzymatic	~ 97.133 μA μM^{-1} cm^{-2}	147.54 nM	- [96]
ZnO nanocones	Hydrazine	Non-enzymatic	50 × 10^4 μA μM^{-1} cm^{-2}	0.01 μM	10 - 100 nM [97]
PVDF-HFP functionalized ZnO thin-film	Hydrazine	Non-enzymatic	-	0.01 nM	- [98]
Au NPs-ZnO-Co_3O_4	Hydrazine	Non-enzymatic	0.058 and 0.048 μA μM^{-1}	-	2–1900 μM and 1900–8500 μM [99]
Ag-doped ZnO	Phenyl Hydrazine	Non-enzymatic	~557.108 ± 0.012 mA (mol L^{-1})$^{-1}$ cm^{-2}	~5 × 10^{-9} mol L^{-1}	- [100]
In-dopped ZnO	Phenyl Hydrazine	Non-enzymatic	70.43 μA• mM^{-1} cm^{-2}	0.5 μM	0.5 μM – 5 mM [101]
ZnO nano-peanuts	Picric Acid	Non-enzymatic	493.64 μA mM^{-1} cm^{-2}	0.125 mM	1 – 5 mM [102]
ZnO-g-CN	4-NT DNT	Non-enzymatic	3.14 μA μM^{-1} cm^{-2}	100 nM 110 nM	1 – 10 μM [103]

(*continued on next page*)

Table 1 (*continued*)

Nanomaterial	Analytes	Approach	Sensitivity	Detection limit	Linear Range [Ref]
			2.28 μA μM^{-1} cm^{-2}		
ZnO-MoS_2	TNT	Non-enzymatic	1.55μA ppm^{-1}	5.2 × 10^{-5} ppm	1 × 10^{-4} - 1 ppm [104]
ZnO@C/GF	TNT	Non-enzymatic	-	3.3 nM	0.1 - 32.2 μM [105]
ZnO nanoglobules-GO based MI-FET	Cr^{3+}	Non-enzymatic	49.28 mA $\mu M^{-1}cm^{-2}$	7.05 μM	10 - 100 μM [106]
ZnO nanoglobules-rGO based MI-FET	Cu^{2+}		185.32 mA μM^{-1} cm^{-2}	14.9 μM	
ZnO nanofibers functionalized by L-cysteine	Pb^{2+}	Non-enzymatic	-	0.397 μg L^{-1}	10 - 140 μg L^{-1} [107]
Phosphate-ZnO	Cd^{2+}	Non-enzymatic	-	4.2 nM	3 - 21 μM [108]
	Hg^{2+}			2.9 nM	
Co doped ZnO-rGO nanorods	Cd^{2+}	Non-enzymatic	-	0.94μg L^{-1}	10-90 μg L^{-1} [109]
	Pb^{2+}			0.83μg L^{-1}	
ZnO-GO	Cr^{3+}	Non-enzymatic	~49.28 mA μM^{-1} cm^{-2}	~7.05 μM	- [110]
ZnO-rGO	Cu^{2+}		~185.32 mA μM^{-1} cm^{-2}	~14.9 μM	

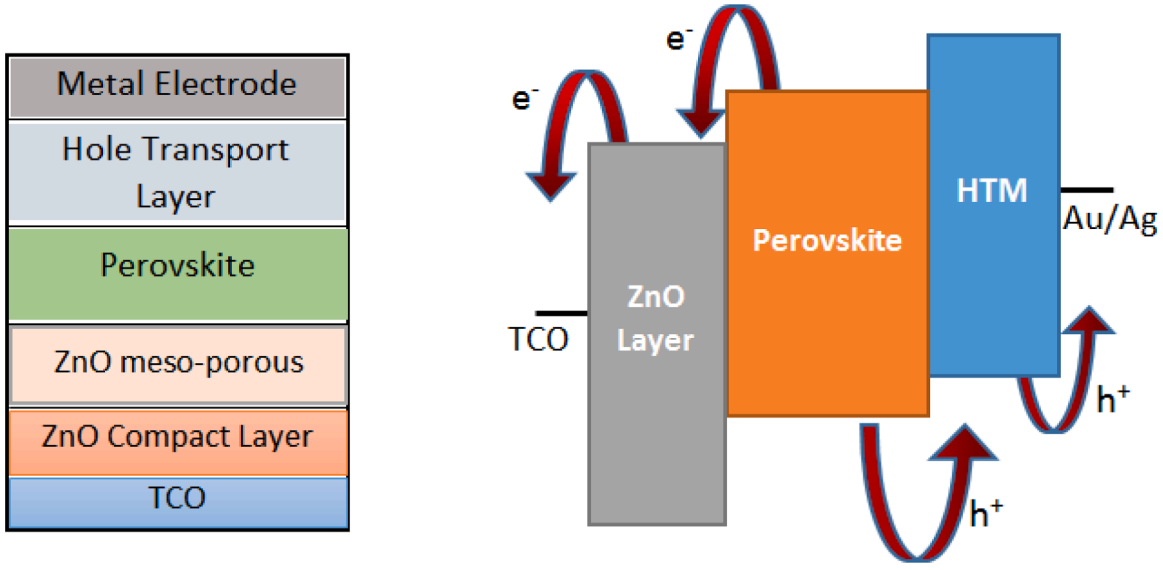

Fig. 7. Typical device structure and carrier transport mechanism of ZnO based perovskite solar cell.

efficiency. These results enlighten the use of doped ZnO in perovskite solar cells and by controlling the doping concentration the efficiency can be improved significantly. ***Song et al.*** [120] studied the effect of annealing temperature on the performance of perovskite solar cells. It was reported that at annealing temperature of 95°C the highest power conversion efficiency of ~18.9% was achieved. Till now this is the highest obtained efficiency for low-temperature processed ZnO nano-rod array based PSCs. The high durability and the stability was the important characteristics for these low temperature processed solar cells which will lead to commercialize the products in near future.

ZnO is a wide bandgap inorganic semiconductor having an electron mobility of 205–300 $cm^2 \bullet V \bullet s^{-1}$ and electron diffusion coefficient of 1.7 × 10^{-4} $cm^2 \bullet s^{-1}$ which is quite higher than TiO_2 [121]. ZnO can be deposited in a various types of nanostructures like nanotubes [122], nanorods [123], nanoparticles [124], nanowires [125], nanobelts [126] and nanosheets [127].

Planar PSCs deposited in between HTL and ETL layer attracted attention among the research community due to their easy fabrication process and capability to be deposited on the flexible substrates [128]. ***Liu and Kelly*** [129] first discussed about the highly efficient ZnO ETL based PSCs having efficiency nearly around 15.7%. The ZnO nanoparticles deposited by spin coating at low temperature possess excellent electron transport property. The ZnO layer deposited was thinner in comparison with mesoporous TiO_2 layer. Also the same research group prepared flexible solar cell using ZnO having an efficiency around 10%. ZnO nanoparticles at low temperature are also prepared by sol-gel method as described by ***Kim et al.*** [130]. Due to the modification of electronic structure of ZnO, the V_{oc} has been improved upto 1.03 volt with a device efficiency of 12.2%. The increase in the V_{oc} is mainly due to the modification of the interfacial layers attached with ZnO which in turn reduces the trap assisted charge recombination in the bulk perovskite layer. The obtained results indicate a new strategy for the researchers to improve the efficiency of the PSCs by modifying the interface of the solar cells.

The properties of ZnO nanoparticles prepared at low temperature mainly depend on the particle size and the layer thickness. Nonetheless, precise control of the above parameters is quite difficult [131]. ZnO layer for the application in PSCs were also prepared by several vacuum based methods. ***Tseng et al.*** [132] prepared ZnO ETL by RF magnetron sputtering technique. The chamber environment can play a significant role on the quality of the deposited ZnO films and in turn the photovoltaic performance of the perovskite solar cell. A very precise control of the surface property of the ZnO is resulting in a better photo conversion efficiency coming ~ 15.9% for the PSCs. Sputtering can be a suitable method to prepare ZnO films with a better control on the properties. Atomic layer deposition (ALD) is another vacuum based widely acceptable technique for the deposition of uniform ZnO layers on a large surface area at a low temperature. ***D. Xu et al.*** [133] reported a device having ZnO deposited by ALD having an efficiency of 13.1%. In this work, the authors have deposited ZnO for the application is PSCs by ALD

method at 70°C. Low temperature processing is an irresistible trend for ALD which leads to develop commercial, large area solar cells.

ZnO nanostructures are widely used metal oxide layers in the application of PSCs due to their high porosity, effective hole blocking capability and high surface area [134]. Though the surface area of the nanorods can be modified by increasing their length and thickness but the efficiency enhancement is not upto the mark till now. Several research groups have studied the impact of a thin ZnO layer along with ZnO nanorods on the performance of PSCs. ***Son et al.*** [135] prepared vertically aligned and tilted nanorods from colloidal and solution based seed layers. It is found that more V_{oc} is obtained from vertically aligned ZnO nanorods. The efficiency achieved was 14.35% after a precise control on the ZnO seed layer and the interface between the ZnO nanorods and perovskite layer. This work emphasized on the fact that the seed layer plays a crucial role on the growth of ZnO nanorods and its alignment which in turn impacts the efficiency. High charge recombination at the interface is a bottleneck for for achieving higher efficiency in the ZnO nanostructure based solar cells. High quality ZnO nanostructures were prepared by several vacuum and non-vacuum methods. Among them hydrothermal [136], electrochemical deposition [137], electrospray [138], PECVD [139] are the widely researched techniques. ***Dong et al.*** [140] investigated the highly efficient Al doped ZnO nanorod developed from sol gel technique for the application in PSCs. It is reported that the interfacial engineering with ZnO:Al leads to enhance the V_{oc} upto a certain limit and the efficiency has enhanced to 10.7%. This study gives an idea regarding doping of ZnO nanostructures and its influence on the performance on PSCs. Several other researchers also studied the effect of doping on ZnO nanostructures and obtained a PCE of PSCs as 12% [141], 16.1% **[119]** and 18.24% [142] for Al, N_2 and I_2 doped ZnO nanorod arrays. ***Dong et al.*** [128] reported the use of Mg doped ZnO nanorod to be used as ETL in the PSCs. By controlling the doping level of Mg, the the energy band levels can also be controlled. The photo conversion efficiency of the cell also significantly improved due to less carrier recombination at the interface. ***Zheng et al.*** [142] demonstrated the deposition of I_2 doped ZnO nano pillars by spin coating method. Due to the suppression of 1D ZnO in the [001] direction by iodine doping, dense and aligned 1D nano pillar structure was formed. The deposited ZnO:I nano pillars shows better optical characteristics in comparison with undoped ZnO structure. The efficiency obtained has reached upto 18.24%. This study actually provides an idea to develop doped ZnO nano pillar with a better orientation which in turn leads to obtain a better efficiency.

From the previous research studies it is evident that the perovskite solar cells have the potential to replace the conventional solar cells. But the long term stability of the perovskite layer is always a matter of concern for the research community and the same need to be investigated and addressed properly [143]. One of the major drawbacks of the perovskite layer on the top of ZnO layer is the thermal instability. It is a common phenomenon that the brown/ black perovskite layer deposited on the ZnO layer turns yellow during the annealing process indicating a rapid degradation after the temperature rises above 95°C [144]. As a whole ZnO is one of the best promising ETL which can replace TiO_2 in terms of low cost, material availability and low temperature processing technology. The ability to prepare ZnO at low temperature enables it to be used on flexible substrates and allows to be deposited on large surface areas. But in spite of these advantages, the instability of perovskite on ZnO layer is still a matter of concern for the application in the PSCs. So a deep understanding of the perovskite material and its preparation on ZnO is required on a large scale.

3.2. In Dye sensitized solar cell (DSSC)

DSSC is growing interest among the researchers due to low fabrication cost, stable operation, good temperature stability and non-toxic emission. Apart from this, DSSC has some more added advantages like wide flexibility in design and very rapid enhancement in efficiency. Inclusion of metal oxide nano-composites in the DSSC solar cell can improve the efficiency and the application potential in many folds. ZnO nano-structures are one of the promising metal composites for the application in DSSC solar cell. **Fig. 8.** depicts the typical device structure and the working methodology of ZnO nano-structure based DSSC.

Several research groups are currently working on ZnO and TiO_2/ZnO nano structures for the application in DSSCs. ***Hsu et al.*** [145] studied the characteristics of sol-gel developed $CuMnO_2$ coated ZnO nanorods for photo-sensing applications. The length of the nanorod were about 1200 nm with a diameter of 60 – 200 nm. The nanorods were having orientation along the c-axis with (002) plane. ***Angaiah et al.*** [146] reported the performance of DSSC based on ZnO nanoparticles and ZnO nanowires. It was reported that the ZnO nanowire based DSSC showed better performance than ZnO nanoparticles due to the least effect of electron hopping which in turn limits the electron transport. The nanowire based DSSC showed power conversion efficiency of 1.81% which is better than the efficiency of nano particle based DSSC~1.13%. ***Bhattacharyya et al.*** [147] studied the effect of doping on ZnO nanowires for the application in DSSC. They reported the deposition of vertically aligned ZnO:Al nanowires for the application on DSSCs at different concentration of Al. The surface morphological and optical characteristics confirmed the preparation of highly transparent and well oriented ZnO nanorods with a hexagonal structure. It was reported that the short circuit current (J_{sc}) improves to 4.4 $mA.cm^{-2}$ for the ZnO:Al based DSSC in comparison with 1.3 $mA.cm^{-2}$ for ZnO based DSSC. The overall power conversion efficiency has also improved up to 0.49% for ZnO:Al nanowire based cell as compared to 0.13% for bare ZnO nanowire based cell. ***Hu et al.*** [148] demonstrated the growth of ZnO nanowire arrays on Ga doped ZnO for the application as photoanode in the DSSCs. The PCE was obtained 1.44% for Ga doped ZnO based DSSC which is better than the efficiency obtained with ZnO nanowires only. The reason for the enhancement in the efficiency is due to high conductivity, better carrier mobility, thermal stability and better surface interface among the layers. It was also found that with the increase in surface area there is an enhancement of the efficiency. ***Jiang et al.*** [149] developed the ZnO nanoflower based photoanode where the material was grown using hydrothermal method at a temperature of 95°C. It was found that the efficiency achieved by ZnO nanoflowers are around 1.9% which is 90% better than the ZnO nanorods. The performance enhancement is mainly due to the light harvesting at ZnO based nanoflower films. This manuscript majorly emphasizes on the application of ZnO nanoflowers for the application of DSSCs. ***Law et al.*** [150] analyzed the performance of DSSCs having ZnO nanowires coated with Al_2O_3 or TiO_2. Bith the alumina and titania shells are improving the open circuit voltage (V_{oc}) but the loss in the short circuit current (J_{sc}) is quite high for alumina. In their research article they reported a ZnO nanowire based DSSC having a conversion efficiency upto 2.25% having titania as outer shell. By improving the surface area of ZnO nanowires or nanorods the performance of the DSSC can be improved significantly. Normally, the reported efficiency of ZnO based DSSC is less than the TiO_2 based DSSCs. The reason behind is that degradation of ZnO in dye environments. So several research groups are working on ZnO/ TiO_2 combination to improve the PCE of DSSCs. ***Xu et al.*** [151] developed TiO_2 coated ZnO nanowire arrays for the application in DSSC and the efficiency ramps up to 5.65% due to the reduction in series resistance. The TiO_2 coated ZnO layer having a thickness of 50 μm is working as better HTMs. ***Chou et al.*** [152] studied the ZnO coated TiO_2 electrodes for the application in DSSC. The electrodes were prepared by spin coating followed by dip coating at a temperature of 70°C. The researchers were able to obtain a highest photo conversion efficiency of 6.62% which is quite higher than the previously reported efficiency of 5.54% by using a TiO_2 electrode only. The enhancement in the efficiency is due to the impact of ZnO barrier and the chemical treatment performed by $TiCl_4$. This research mainly emphasized on the feasibility of the use of ZnO coated TiO_2 electrodes on the DSSC to improve the performance and the stability. A summary of the reported ZnO nano-structured based devices in photovoltaic applications was

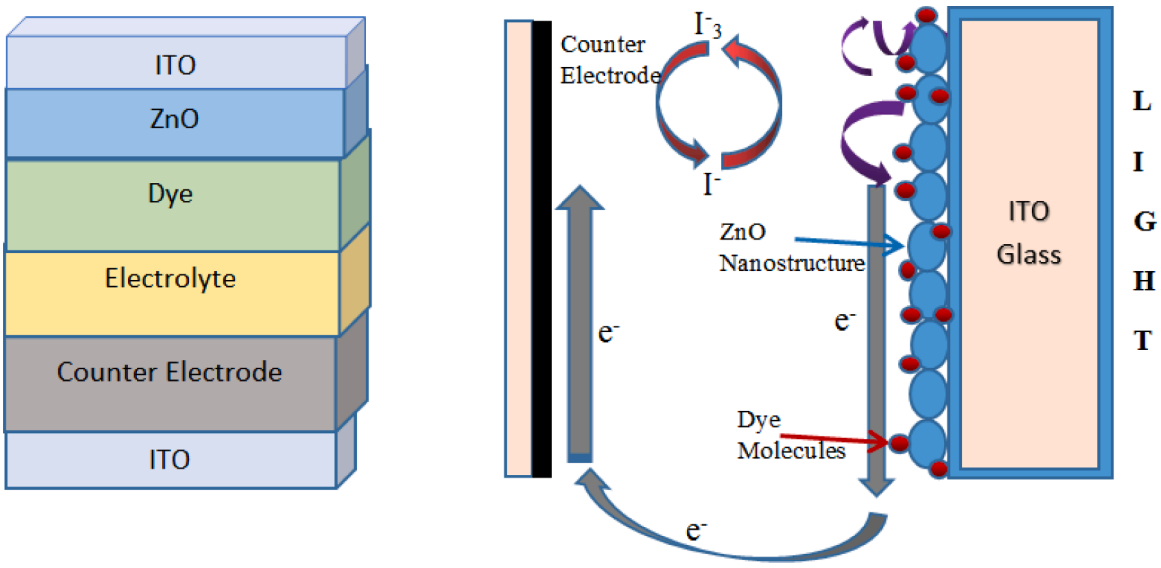

Fig. 8. The device structure and the working methodology of ZnO nanostructure based DSSC.

summarized in Table 2.

3.3. In UV photodetectors

Apart from the application in perovskite and dye sensitized solar cells, ZnO nano-structures were also used for UV Photodetectors. UV photodetectors fabricated from1D ZnO nanostructures are gaining lot of interest among the researchers. The performance of ZnO based nano-structured photo detectors can further be improved by doping metal nanoparticles on the surface of the same. ***Li et al.*** [153] studied the sensing of UV light using ZnO nanorod with the structure ZnO/PEDOT/HfO_2/GaN. The deposited ZnO nanorods have a very sharp hexagonal structure, with a height of 14 μm. The preferential orientation was (0002) with hexagonal wurtzite structure. ***Rakhsha et al.*** [154] reported the solution based fabrication of ZnO nano arrays for the application of UV sensing. Doping of different other metals like Ga, Ag and Cu was done to study the effect of doping on the sensing properties. From the obtained results it can be concluded that the incorporation of Ga reduces the rectifying ratio (RR), whereas the maximum RR is obtained for undoped and Cu doped ZnO with a value of 12.7. The performance of the same device enhanced upto 50% as compared to other devices when exposed to UV light. ***Li et al.*** [155] studied the performance of photodetector having the composition of ZnO nanowall/Ag nanowire. The UV detectors having ZnO nanowall/Ag nanocomposite showed higher response time (S=285) and less response-recovery time (10s, 81s). It can be concluded from the obtained results that ZnO nanocomposites associated with Ag is a promising device for better UV sensing. ***Singh et al.*** [156] in their work reported the UV detection parameters for ZnO nanorods based devices. The substrate used for their research work is Si and the development of the ZnO nanorods was done in two steps. The fabricated device having the structure Pd/ZnO-NR's/Pd show a very good response when exposed to UV. This study will be very helpful for the fabrication of ZnO nanorods in hydrothermal technique for UV detection. ***Eom et al.*** [157] studied the performance of ZnO nanorods based UV sensors developed hydrothermally on Polyethylene terephthalate (PET). The authors have studied the characteristics of the device with the change in seed solution to growth solution. It was found that by optimizing the ratio of seed to growth solution the best UV sensing properties can be obtained. ***Guo et al.*** [158] reported the detection of UV using ZnO nanowires deposited using dielectrophoresis technique. The responsivity of the device was obtained upto 40 A/W at 10 V bias. ***Kar et al.*** [159] reported the groeth of ZnO nanowires using CVD on Si substrates. The photosensitivity of the fabricated device was studied and it was found that the nanowires grown on bottom surface showed better UV response. ***Nasiri et al.*** [160] designed a portable visible-blind UV photodetectors using ZnO nanostructures. The device showed a very high sensitivity with a very high output current when the input UV radiation intensity was quite less. Several other researchers have studied the effect of adding metals with ZnO nanostructures to improve its UV sensing properties. ***Mohammad et al.*** [161] developed Ag nanoparticle encapsulated ZnO nanorods arrays on Si substrates. The authors observed a notable change on the surface with the incorporation of Ag nanoparticles. With the addition of Ag nanoparticles the electrical properties enhanced in comparison with ZnO nanorod without Ag nanoparticle. The final device fabricated shows a device sensitivity of 18503% which allows the device a suitable option for self-powered photodetectors. ***Abbasi et al.*** [162] studied the UV detector response of ZnO and ZnO:Ni nanostructure devices having different Ni concentration. Metal-semiconductor-metal (MSM) structure was used to fabricate the UV photo detectors. It was found that the ZnO:Ni nanostructure based photodetectors showed a better response in comparison to pure ZnO based devices. The best response found was 0.5s for rise time and 2s decay time having 7% Ni concentration. ***Liu et al.*** [163] deposited Tellurium dioxide (TeO_2) doped zinc oxide (ZnO) nanorods by chemical vapor deposition technique on Si substrates being covered by Au film. The TeO_2 content has been modulated to study the impact on UV photo detection. It is found that with the variation of TeO_2 content, the fabricated devices are capable of sensing UV and NIR also. ***Sahatiya et al.*** [164] demonstrated the development of black phosphorous on ITO substrates, encapsulated with ZnO which can be a suitable device for the detection of UV lights. The developed ZnO on the black phosphorous surface have shown several suitable characteristics like long term stability and improvement of spectral absorbance in the UV region. This research shows a path of using black phosphorous as a passivation material grown on different substrates having ZnO layer for the application in the field of optical sensors. In another work, this research group has developed a Gr/ZnO heterojunction on flexible substrate by hydrothermal technique to detect UV light at room temperature. By inducing strain, piezopotential is developed for the fabricated device and the photosensing was enhanced by 87% with the applied strain. The result shown here provides a detailed understanding of the improvement of the optoelectronic performance of Gr/ZnO interface which will help the research community to apply the same understanding in other hetero-junction also [165].

Table 2
List of ZnO nano-structured based devices in photovoltaic applications.

Perovskite Solar Cell Sl. No.	Device Structure	ZnO Nano Structure	Short Circuit Current Density (J_{sc}) mA/cm^2	Open Circuit Voltage (V_{oc}) Volt	Fill Factor (FF) %	Efficiency (η) %	Ref.
1.	ITO/ZnO/PTB7:$PC_{71}BM$/MoO_3/Ag	Nanoparticles	15.78	0.73	62.18	7.16	[116]
2.	FTO/ZnO/PbI_2/CH_3NH_3I/HTM/Au	Nanorods	20.9	0.991	56	11.13	[118]
3.	ITO/ZnO-NR/$MAPbI_3$/Spiro-OMeTAD/Ag	Nanorods	21.5	0.964	70	16.12	[119]
4.	ITO/ZnO/Cs10M/spiro-OMeTAD/Ag	Nanoparticles	22.5	1.11	71.7	17.9	[120]
5.	ITO/NiO_x/ $CH_3NH_3PbI_3$/PCBM/ZnO/Ag	Nanoparticles	19.67	1.04	78.23	16	[124]
6.	FTO/ZnO/$CH_3NH_3PbI_3$/Metal Contact	Nanowires	14.30	0.879	56.1	7.05	[125]
7.	FTO/ZnO/$CH_3NH_3PbI_3$/ Spiro-OMeTAD/Ag	Nano sheets	21.0	0.980	70	14.40	[127]
8.	ITO/ZnO/$CH_3NH_3PbI_3$/ Spiro-OMeTAD/Ag	Nanoparticles	20.4	1.03	74.9	15.7	[129]
9.	Glass/ITO/ZnO/ $CH_3NH_3PbI_3$/PTB7-$ThMoO_3$/Ag	-	14.73	1.02	73	10.87	[130]
10.	FTO/ZnO/ $CH_3NH_3PbI_3$/ spiro-MeOTAD/Au	Nanorods	20.40	0.956	59.9	11.68	[135]
11.	ITO/PEDOT:PSS/$CH_3NH_3PbI_{3-x}Cl_x$/$PC_{61}BM$/ZnO-NRs/Ag	Nanorods	19.72	1.09	76.69	16.55	[136]
12.	FTO/ZnO/i-ZnO/ $CH_3NH_3PbI_3$/spiro-MeOTAD/Ag	Nanowires	21.9	0.99	47.3	10.28	[137]
13.	FTO/ZnO/ZnO:Al/$CH_3NH_3PbI_3$/spiro-MeOTAD/Ag	-	16.0	1.010	67.0	10.8	[138]
14.	FTO/ZnO/ZnO:Al/$CH_3NH_3PbI_3$/spiro-MeOTAD/Ag	Nanorods	19.77	0.900	60	10.7	[140]
15.	FTO/ZnO:Mg/$CH_3NH_3PbI_3$/Contact	Nanorods	22.7	0.990	68	15.3	[141]
16.	ITO/ZnO:I/$CH_3NH_3PbI_3$/spiro-MeOTAD/Ag	Nanopillars	22.42	1.13	71.99	18.24	[142]
Dye Sensitized Solar cell							
Sl. No.	**Electrode Specification**	**ZnO Nano Structure**	**Short Circuit Current Density (J_{sc})**	**Open Circuit Voltage (V_{oc})**	**Fill Factor (FF)**	**Efficiency**	**Ref.**
17.	Photoanode (ZnO) and Counter Electrode (Pt)	Nanoparticles	4.31	0.55	47.5	1.13	[146]
18.	Photoanode (ZnO) and Counter Electrode (Pt)	Nanowires	6.64	0.58	46.9	1.81	[146]
19.	Photoanode (ZnO and ZnO:Al) and Counter Electrode (FTO)	Nanowires	4.4	0.28	40	0.49	[147]
20.	Photoanode (ZnO:Ga) and Counter Electrode (Pt)	Nanowires	4.03	0.61	59	1.44	[148]
21.	Photoanode (ZnO)	Nanoflower	5.5	0.65	53	1.9	[149]
22.	Photoanode (ZnO)	Nanorods	4.5	0.63	36	1.0	[149]
23.	Photoanode (ZnO-Al_2O_3 and ZnO-TiO_2) and Counter Electrode (Pt)	Nanowires	4.45	0.56	42	1.05	[150]
24.	Photoanode (TiO_2-coated ZnO)	Nanowires	12.4	0.798	59.4	5.86	[151]
25.	Photoanode (TiO_2-coated ZnO) and Counter Electrode (Pt)	-	13.46	0.75	65.4	6.62	[152]

4. Conclusion and outlook

This review summarizes the properties, and applications of ZnO in sensors towards biomedical, optical and environmental monitoring using the electro-chemical and FET based sensing methods. These wide-ranging applications of ZnO mainly originate from its brilliant opto-electronic, physico-chemical, electrical properties such as, low dielectric constant, plentiful Zn-O bonds, high luminous transmittance, good stability, huge excitation binding energy, large surface area to volume ratio and so on. Since ZnO is mostly synthesized at elevated temperatures, substantial work needs to be done towards the synthesis of ZnO at low temperatures, thus making it compatible to deposit on flexible substrates. Secondly, since the performance of the ZnO based sensors is influenced by its morphology to a large extent, distinctive synthesis methods are anticipated to control the desired shape and size of ZnO for achieving better sensitivity. For example, 2D ZnO exhibits large specific surface area that offers enormous number of active sites for surface functionalization of analytes, thus endorsing the repeatability of a sensor. In the last part of the review, the application of ZnO nanostructures for optical sensing was conferred. It was found that the application of ZnO nanostructures in the perovskite and dye sensitized solar cells modified its efficiency. ZnO nano-structures based devices for UV detection were also discussed. It was found that doping ZnO with different metals improves the sensitivity of detection. To conclude, different types of ZnO nanostructures such as nanorods, nanoarrays, nanoflowers, nanowires are widely researched and applied for various types of sensing applications. Though, all these sensors displayed decent performances, most of these developments are merely proof-of-concept demonstrations and limited to lab-based research endeavors. Therefore, to commercialize the ZnO based sensors, consolidation of this sensing platform into device level is indispensible with the assistance of robust interfacing electronics. In this respect, current research towards the fabrication of low-priced paper based 'one-time use' sensors or flexible FET type devices for recognition of analytes exhibits enormous prospects. Exciting progressions are predicted soon to materialize ZnO based scalable sensing systems and testing tools.

CRediT authorship contribution statement

Rinky Sha: Conceptualization, Resources, Data curation, Writing – original draft, Writing – review & editing. **Arindam Basak:** Conceptualization, Resources, Data curation, Writing – original draft, Writing – review & editing. **Palash Chandra Maity:** Conceptualization, Resources, Data curation, Writing – original draft, Writing – review & editing. **Sushmee Badhulika:** Writing – review & editing.

Declaration of Competing Interest

The authors declare that they have no known competing financial interests or personal relationships that could have appeared to influence the work reported in this paper.

References

[1] W. Yan, H. Xu, M. Ling, S. Zhou, T. Qiu, Y. Deng, E. Zhang, MOF-derived porous hollow Co3O4@ ZnO cages for high-performance MEMS trimethylamine sensors, ACS Sens. 6 (7) (2021) 2613–2621.

[2] X. He, Y. Liu, Y. Liu, S. Cui, W. Liu, Z. Li, Controllable fabrication of Ag-NP-decorated porous ZnO nanosheet arrays with superhydrophobic properties for high performance SERS detection of explosives, Cryst. Eng. Comm. 22 (4) (2020) 776–785.

[3] R. Sha, S. Badhulika, A. Mulchandani, Graphene-based biosensors and their applications in biomedical and environmental monitoring. Label-free biosensing, Springer, Cham, 2017, pp. 261–290.

[4] R. Sha, S.S. Jones, N. Vishnu, B. Soundiraraju, S. Badhulika, A novel biomass derived carbon quantum dots for highly sensitive and selective detection of hydrazine, Electroanalysis 30 (10) (2018) 2228–2232.

[5] R. Sha, A. Gopalakrishnan, K.V. Sreenivasulu, V.V. Srikanth, S. Badhulika, Template-cum-catalysis free synthesis of α-MnO2 nanorods-hierarchical MoS2 microspheres composite for ultra-sensitive and selective determination of nitrite, J. Alloys Compd. 794 (2019) 26–34.

[6] P.C. Maity, N.V. Pulagara, J. Arya, G. Kaur, Y. Khan, I. Lahiri, Nickel oxide-1D/2D carbon nanostructure hybrid as efficient field emitters, J. Mater. Sci. Mater. Electron. (2021) 1–14.

[7] A. Sharma, A. Ahmed, A. Singh, S. Oruganti, A. Khosla, S. Arya, Recent advances in tin oxide nanomaterials as electrochemical/chemiresistive sensors, J. Electrochem. Soc. (2021).

[8] A. Sett, S. Dey, P.K. Guha, T.K. Bhattacharyya, ZnO/$\gamma $-Fe 2 O 3 heterostructure toward high-performance acetone sensing, IEEE Sensors J. 19 (19) (2019) 8576–8582.

[9] A. Sett, M. Mondal, T.K. Bhattacharyya, Hierarchical ZnO nanorods with tailored surface defects for enhanced acetone sensing, IEEE Sensors J. 19 (10) (2019) 3601–3608.

[10] A. Sett, A.K. Mukhopadhyay, M. Mondal, S. Majumder, T.K. Bhattacharyya, Tuning surface defects of mesoporous ZnO nanorods for high speed humidity sensing application, in: 2018 IEEE SENSORS, IEEE, 2018, pp. 1–4.

[11] Rajeshwari Garain, Arindam Basak, Udai P. Singh, Study of thickness and temperature dependence on the performance of SnS based solar cell by SCAPS-1D, Mater. Today: Proc. 39 (2021) 1833–1837.

[12] Lucio Claudio Andreani, Angelo Bozzola, Piotr Kowalczewski, Marco Liscidini, Lisa Redorici, Silicon solar cells: toward the efficiency limits, Adv. Phys.: X 4 (1) (2019), https://doi.org/10.1080/23746149.2018.1548305.

[13] Allon I. Hochbaum, Peidong Yang, Semiconductor Nanowires for Energy Conversion, Chem. Rev. 110 (1) (2010) 527–546.

[14] A. Basak, A. Mondal, U.P. Singh, Post-growth annealing effect on the performance of Cu2SnSe3 solar cells, Mater. Res. Express 5 (10) (2018), 105505.

[15] A. Basak, A. Hati, A. Mondal, U.P. Singh, S.K. Taheruddin, Effect of substrate on the structural, optical and electrical properties of SnS thin films grown by thermal evaporation method, Thin. Solid. Films 645 (2018) 97–101.

[16] Z. Yang, M. Wang, X. Song, G. Yan, Y. Ding, J. Bai, High-performance ZnO/Ag Nanowire/ZnO composite film UV photodetectors with large area and low operating voltage, J. Mater. Chem. C 2 (21) (2014) 4312–4319.

[17] K.Y. Goud, K.K. Reddy, M. Satyanarayana, S. Kummari, K.V. Gobi, A review on recent developments in optical and electrochemical aptamer-based assays for mycotoxins using advanced nanomaterials, Microchim. Acta 187 (1) (2020) 1–32.

[18] R. Sha, A. Kadu, K. Matsumoto, S. Uno, S. Badhulika, Ultra-low cost, smart sensor based on pyrite FeS2 on cellulose paper for the determination of vital plant hormone methyl jasmonate, Eng. Res. Express 2 (2) (2020), 025020.

[19] M.B. Kulkarni, P.K. Enaganti, K. Amreen, S. Goel, Integrated temperature controlling platform to synthesize ZnO nanoparticles and its deposition on Al-foil for biosensing, IEEE Sensors J. 21 (7) (2021) 9538–9545.

[20] J. Gao, B. Wu, C. Cao, Z. Zhan, W. Ma, X. Wang, Unraveling the dynamic evolution of Pd species on Pd-loaded ZnO nanorods for different hydrogen sensing behaviors, ACS Sustain. Chem. Eng. 9 (18) (2021) 6370–6379.

[21] B. Ortiz-Casas, A. Galdámez-Martínez, J. Gutiérrez-Flores, A.B. Ibañez, P. K. Panda, G. Santana, A. Dutt, Bio-acceptable 0D and 1D ZnO nanostructures for cancer diagnostics and treatment, Mater. Today (2021).

[22] S. Demirezen, H.G. Çetinkaya, M. Kara, F. Yakuphanoğlu, Ş. Altındal, Synthesis, electrical and photo-sensing characteristics of the Al/(PCBM/NiO: ZnO)/p-Si nanocomposite structures, Sens. Actuators A 317 (2021), 112449.

[23] Y. Li, W. Wang, H. Gong, J. Xu, Z. Yu, Q. Wei, D. Tang, Graphene-coated copper-doped ZnO quantum dots for sensitive photoelectrochemical bioanalysis of thrombin triggered by DNA nanoflowers, J. Mater. Chem. B 9 (34) (2021) 6818–6824.

[24] M. Lei, M. Gao, X. Yang, Y. Zou, A. Alghamdi, Y. Ren, Y. Deng, Size-Controlled Au Nanoparticles Incorporating Mesoporous ZnO for Sensitive Ethanol Sensing, ACS Appl. Mater. Interfaces (2021).

[25] R. Sha, S.K. Puttapati, V.V. Srikanth, S. Badhulika, Ultra-sensitive non-enzymatic ethanol sensor based on reduced graphene oxide-zinc oxide composite modified electrode, IEEE Sensors J. 18 (5) (2017) 1844–1848.

[26] A. Czyżowska, A. Barbasz, A review: zinc oxide nanoparticles–friends or enemies? Int. J. Environ. Health Res. (2020) 1–17.

[27] R. Verma, S. Pathak, A.K. Srivastava, S. Prawer, S. Tomljenovic-Hanic, ZnO Nanomaterials: Green synthesis, toxicity evaluation and new insights in biomedical applications, J. Alloys Compd. (2021), 160175.

[28] K. Gold, B. Slay, M. Knackstedt, A.K. Gaharwar, Antimicrobial activity of metal and metal-oxide based nanoparticles, Adv. Therapeutics 1 (3) (2018), 1700033.

[29] J.H. Luo, Q. Liu, L.N. Yang, Z.Z. Sun, Z.S. Li, First-principles study of electronic structure and optical properties of (Zr–Al)-codoped ZnO, Comput. Mater. Sci. 82 (2014) 70–75.

[30] E. Nurfani, W.A.P. Kesuma, A. Lailani, M.S. Anrokhi, G.T.M. Kadja, M. Rozana, M. F. Arif, Enhanced UV sensing of ZnO films by Cu doping, Opt. Mater. 114 (2021), 110973.

[31] E.I. Naik, H.B. Naik, M.S. Sarvajith, E. Pradeepa, Co-precipitation synthesis of cobalt doped ZnO nanoparticles: characterization and their applications for biosensing and antibacterial studies, Inorg. Chem. Commun. 130 (2021), 108678.

[32] Q.A. Drmosh, Y.A. Al Wajih, I.O. Alade, A.K. Mohamedkhair, M. Qamar, A. S. Hakeem, Z.H Yamani, Engineering the depletion layer of Au-modified ZnO/Ag core-shell films for high-performance acetone gas sensing, Sens. Actuators B 338 (2021), 129851.

[33] S.S. Bhat, A. Qurashi, F.A. Khanday, ZnO nanostructures based biosensors for cancer and infectious disease applications: Perspectives, prospects and promises, TrAC Trends Anal. Chem. 86 (2017) 1–13.

[34] R. Sha, T.K. Bhattacharyya, MoS2-based nanosensors in biomedical and environmental monitoring applications, Electrochim. Acta 349 (2020), 136370.

[35] R. Sha, S. Badhulika, Recent advancements in fabrication of nanomaterial based biosensors for diagnosis of ovarian cancer: a comprehensive review, Microchim. Acta 187 (3) (2020) 1–15.

[36] P. Sahatiya, R. Sha, S. Badhulika, Flexible 2D electronics in sensors and bioanalytical applications. Handbook of Flexible and Stretchable Electronics, 2019.

[37] R. Sha, S. Badhulika, Facile green synthesis of reduced graphene oxide/tin oxide composite for highly selective and ultra-sensitive detection of ascorbic acid, J. Electroanal. Chem. 816 (2018) 30–37.

[38] D. Feng, J. Su, Y. Xu, G. He, C. Wang, X. Wang, X. Mi, DNA tetrahedron-mediated immune-sandwich assay for rapid and sensitive detection of PSA through a microfluidic electrochemical detection system, Microsyst. Nanoeng. 7 (1) (2021) 1–10.

[39] D. Chen, X. Zou, F. Dong, C. Zhen, D. Xiao, X. Wang, J. Tu, Donor–acceptor compensated ZnO semiconductor for photoelectrochemical biosensors, ACS Appl. Mater. Interfaces (2021).

[40] S. Badhulika, R.K. Paul, T. Terse, A. Mulchandani, Nonenzymatic glucose sensor based on platinum nanoflowers decorated multiwalled carbon nanotubes-graphene hybrid electrode, Electroanalysis 26 (1) (2014) 103–108.

[41] R. Sha, L. Durai, S. Badhulika, Facile in-situ preparation of few-layered reduced graphene oxide–niobium pentoxide composite for non-enzymatic glucose monitoring, in: 2018 4th IEEE International Conference on Emerging Electronics (ICEE), IEEE, 2018, pp. 1–4.

[42] S. Baruah, B. Maibam, C.K. Borah, T. Agarkar, A. Kumar, S. Kumar, A highly receptive ZnO based enzymatic electrochemical sensor for glucose sensing, IEEE Sensors J. (2021).

[43] J.R. Anusha, H.J. Kim, A.T. Fleming, S.J. Das, K.H. Yu, B.C. Kim, C.J. Raj, Simple fabrication of ZnO/Pt/chitosan electrode for enzymatic glucose biosensor, Sens. Actuators B 202 (2014) 827–833.

[44] N.S. Ridhuan, N.M. Nor, K.A. Razak, Z. Lockman, N.D. Zakaria, ITO electrode modified with Pt nanodendrites-decorated ZnO nanorods for enzymatic glucose sensor, J. Solid State Electrochem. 25 (3) (2021) 1065–1072.

[45] B. Yang, N. Han, S. Hu, L. Zhang, S. Yi, Z. Zhang, Y. Gao, Cu/ZnO nano-thorn with modifiable morphology for photoelectrochemical detection of glucose, J. Electrochem. Soc. 168 (2) (2021), 027516.

[46] A. Awais, M. Arsalan, X. Qiao, W. Yahui, Q. Sheng, T. Yue, Y. He, Facial synthesis of highly efficient non-enzymatic glucose sensor based on vertically aligned Au-ZnO NRs, J. Electroanal. Chem. 895 (2021), 115424.

[47] V. Vinoth, G. Subramaniyam, S. Anandan, H. Valdés, P. Manidurai, Non-enzymatic glucose sensor and photocurrent performance of zinc oxide quantum dots supported multi-walled carbon nanotubes, Mater. Sci. Eng. 265 (2021), 115036.

[48] H. Imran, K. Vaishali, S.A. Francy, P.N. Manikandan, V. Dharuman, Platinum and zinc oxide modified carbon nitride electrode as non-enzymatic highly selective and reusable electrochemical diabetic sensor in human blood, Bioelectrochemistry 137 (2021), 107645.

[49] A.K. Manna, P. Guha, V.J. Solanki, S.K. Srivastava, S. Varma, Non-enzymatic glucose sensing with hybrid nanostructured Cu 2 O-ZnO prepared by single-step coelectrodeposition technique, J. Solid State Electrochem. 24 (7) (2020) 1647–1658.

[50] F. Zhou, Y. Li, Y. Tang, F. Gao, W. Jing, Y. Du, F. Han, A novel flexible non-enzymatic electrochemical glucose sensor of excellent performance with ZnO nanorods modified on stainless steel wire sieve and stimulated via UV irradiation, Ceram. Int. (2022), https://doi.org/10.1016/j.ceramint.2022.01.332.

[51] M. Waqas, C. Liu, Q. Huang, X. Zhang, Y. Fan, Z. Jiang, W. Chen, Zn2+ induced self-assembled fabrication of marigold-like ZnO microflower@ Ni (OH) 2 three-dimensional nanosheets for nonenzymatic glucose sensing, Electrochim. Acta (2022), 140040.

[52] R. Sha, K. Komori, S. Badhulika, Graphene–Polyaniline composite based ultra-sensitive electrochemical sensor for non-enzymatic detection of urea, Electrochim. Acta 233 (2017) 44–51.

[53] R. Ahmad, N. Tripathy, Y.B. Hahn, Highly stable urea sensor based on ZnO nanorods directly grown on Ag/glass electrodes, Sens. Actuators B 194 (2014) 290–295.

[54] R. Rahmanian, S.A. Mozaffari, M. Abedi, Disposable urea biosensor based on nanoporous ZnO film fabricated from omissible polymeric substrate, Mater. Sci. Eng. 57 (2015) 387–396.

[55] K.B. Babitha, P.S. Soorya, A.P. Mohamed, R.B. Rakhi, S. Ananthakumar, Development of ZnO@ rGO nanocomposites for the enzyme free electrochemical detection of urea and glucose, Mater. Adv. 1 (6) (2020) 1939–1951.

[56] J. Yoon, D. Lee, E. Lee, Y.S. Yoon, D.J. Kim, Ag/ZnO catalysts with different ZnO nanostructures for non-enzymatic detection of urea, Electroanalysis 31 (1) (2019) 17–21.

[57] C.S. Kushwaha, P. Singh, N.S. Abbas, S.K. Shukla, Self-activating zinc oxide encapsulated polyaniline-grafted chitosan composite for potentiometric urea sensor, J. Mater. Sci. Mater. Electron. 31 (14) (2020) 11887–11896.

[58] J. Deepika, R. Sha, S. Badhulika, A ruthenium (IV) disulfide based non-enzymatic sensor for selective and sensitive amperometric determination of dopamine, Microchim. Acta 186 (7) (2019) 1–10.

[59] L. Zhihua, Z. Xue, H. Xiaowei, Z. Xiaobo, S. Jiyong, X. Yiwei, Z. Xiaodong, Hypha-templated synthesis of carbon/ZnO microfiber for dopamine sensing in pork, Food Chem. 335 (2021), 127646.

[60] F. Li, B. Ni, Y. Zheng, Y. Huang, G. Li, A simple and efficient voltammetric sensor for dopamine determination based on ZnO nanorods/electro-reduced graphene oxide composite, Surf. Interfaces (2021), 101375.

[61] A.A. Firooz, M. Ghalkhani, J.A.F. Albanese, M. Ghanbari, High electrochemical detection of dopamine based on Cu doped single phase hexagonally ZnO plates, Mater. Today Commun. 26 (2021), 101716.

[62] M. Gu, H. Xiao, S. Wei, Z. Chen, L. Cao, A portable and sensitive dopamine sensor based on AuNPs functionalized ZnO-rGO nanocomposites modified screen-printed electrode, J. Electroanal. Chem. (2022), 116117.

[63] R. Sha, N. Vishnu, S. Badhulika, FeS2 grown pencil graphite as an in-expensive and non-enzymatic sensor for sensitive detection of uric acid in non-invasive samples, Electroanalysis 31 (12) (2019) 2397–2403.

[64] R. Sha, N. Vishnu, S. Badhulika, MoS2 based ultra-low-cost, flexible, non-enzymatic and non-invasive electrochemical sensor for highly selective detection of uric acid in human urine samples, Sens. Actuators B 279 (2019) 53–60.

[65] X. Liu, P. Lin, X. Yan, Z. Kang, Y. Zhao, Y. Lei, Y. Zhang, Enzyme-coated single ZnO nanowire FET biosensor for detection of uric acid, Sens. Actuators B 176 (2013) 22–27.

[66] M. Ali, I. Shah, S.W. Kim, M. Sajid, J.H. Lim, K.H. Choi, Quantitative detection of uric acid through ZnO quantum dots based highly sensitive electrochemical biosensor, Sens. Actuators A 283 (2018) 282–290.

[67] B. Ramya, P.G. Priya, Rapid phytochemical microwave-assisted synthesis of zinc oxide nano flakes with excellent electrocatalytic activity for non-enzymatic electrochemical sensing of uric acid, J. Mater. Sci. Mater. Electron. (2021) 1–19.

[68] M.M. Alam, A.M. Asiri, M.T. Uddin, M.A. Islam, M.R. Awual, M.M. Rahman, Detection of uric acid based on doped ZnO/Ag 2 O/Co 3 O 4 nanoparticle loaded glassy carbon electrode, New J. Chem. 43 (22) (2019) 8651–8659.

[69] R.S. Veerla, P. Sahatiya, S. Badhulika, Fabrication of a flexible UV photodetector and disposable photoresponsive uric acid sensor by direct writing of ZnO pencil on paper, J. Mater. Chem. C 5 (39) (2017) 10231–10240.

[70] M. Eryiğit, B.K. Urhan, H.Ö. Doğan, T.Ö. Özer, Ü. Demir, ZnO nanosheets-decorated ERGO layers: an efficient electrochemical sensor for non-enzymatic uric acid detection, IEEE Sensors J. (2022).

[71] K. Samoson, A. Soleh, K. Saisahas, K. Promsuwan, J. Saichanapan, P. Kanatharana, W. Limbut, Facile fabrication of a flexible laser induced gold nanoparticle/chitosan/porous graphene electrode for uric acid detection, Talanta (2022), 123319.

[72] R. Sha, N. Vishnu, S. Badhulika, Bimetallic Pt-Pd nanostructures supported on MoS 2 as an ultra-high performance electrocatalyst for methanol oxidation and nonenzymatic determination of hydrogen peroxide, Microchim. Acta 185 (8) (2018) 1–11.

[73] S.B. Khan, M.M. Rahman, A.M. Asiri, S.A.B. Asif, S.A.S. Al-Qarni, A.G. Al-Sehemi, M.S. Al-Assiri, Fabrication of non-enzymatic sensor using Co doped ZnO nanoparticles as a marker of H2O2, Physica E 62 (2014) 21–27.

[74] X. Ke, G. Zhu, Y. Dai, Y. Shen, J. Yang, J. Liu, Fabrication of Pt-ZnO composite nanotube modified electrodes for the detection of H2O2, J. Electroanal. Chem. 817 (2018) 176–183.

[75] M.A. Rashed, M. Faisal, F.A. Harraz, M. Jalalah, M. Alsaiari, S.A. Alsareii, A Highly Efficient Nonenzymatic Hydrogen Peroxide Electrochemical Sensor Using Mesoporous Carbon Doped ZnO Nanocomposite, J. Electrochem. Soc. 168 (2) (2021), 027512.

[76] H. Wu, H.Y. Chung, D.C. Tsang, N.M. Huang, Z. Xie, H.N. Lim, Y.H. Ng, Scavenger-free and self-powered photocathodic sensing system for aqueous hydrogen peroxide monitoring by CuO/ZnO nanostructure, Chem. Eng. Sci. 226 (2020), 115886.

[77] M. Haque, H. Fouad, H.K. Seo, O.Y. Alothman, Z.A. Ansari, Cu-doped ZnO nanoparticles as an electrochemical sensing electrode for cardiac biomarker myoglobin detection, IEEE Sensors J. 20 (15) (2020) 8820–8832.

[78] M. Haque, H. Fouad, H.K. Seo, A.Y. Othman, A. Kulkarni, Z.A. Ansari, Investigation of Mn doped ZnO nanoparticles towards ascertaining myocardial infarction through an electrochemical detection of myoglobin, IEEE Access 8 (2020) 164678–164692.

[79] Z.H. Ibupoto, N. Jamal, K. Khun, M. Willander, Development of a disposable potentiometric antibody immobilized ZnO nanotubes based sensor for the detection of C-reactive protein, Sens. Actuators B 166 (2012) 809–814.

[80] S. Dong, D. Zhang, H. Cui, T. Huang, ZnO/porous carbon composite from a mixed-ligand MOF for ultrasensitive electrochemical immunosensing of C-reactive protein, Sens. Actuators B 284 (2019) 354–361.

[81] S. Madhu, A.J. Anthuuvan, S. Ramasamy, P. Manickam, S. Bhansali, P. Nagamony, V. Chinnuswamy, ZnO nanorod integrated flexible carbon fibers for sweat cortisol detection, ACS Appl. Electronic Mater. 2 (2) (2020) 499–509.

[82] B. Chakraborty, R. Saha, S. Chattopadhyay, D. De, R.D. Das, M.K. Mukhopadhyay, C. RoyChaudhuri, Impact of surface defects in electron beam evaporated ZnO thin films on FET biosensing characteristics towards reliable PSA detection, Appl. Surf. Sci. 537 (2021), 147895.

[83] E. Shabani, M.J. Abdekhodaie, S.A. Mousavi, F. Taghipour, ZnO nanoparticle/nanorod-based label-free electrochemical immunoassay for rapid detection of MMP-9 biomarker, Biochem. Eng. J. 164 (2020), 107772.

[84] T. Yang, M. Chen, Q. Kong, X. Luo, K. Jiao, Toward DNA electrochemical sensing by free-standing ZnO nanosheets grown on 2D thin-layered MoS2, Biosens. Bioelectron. 89 (2017) 538–544.

[85] X. Cao, X. Cao, H. Guo, T. Li, Y. Jie, N. Wang, Z.L. Wang, Piezotronic effect enhanced label-free detection of DNA using a schottky-contacted ZnO nanowire biosensor, ACS nano 10 (8) (2016) 8038–8044.

[86] C. Murugan, N. Murugan, A.K. Sundramoorthy, A. Sundaramurthy, Gradient triple-layered ZnS/ZnO/Ta2O5–SiO2 core–shell nanoparticles for enzyme-based electrochemical detection of cancer biomarkers, ACS Appl. Nano Mater. 3 (8) (2020) 8461–8471.

[87] R. Sha, S.K. Puttapati, V.V. Srikanth, S. Badhulika, Ultra-sensitive phenol sensor based on overcoming surface fouling of reduced graphene oxide-zinc oxide composite electrode, J. Electroanal. Chem. 785 (2017) 26–32.
[88] H.B. Balkhoyor, M.M. Rahman, A.M. Asiri, Effect of Ce doping into ZnO nanostructures to enhance the phenolic sensor performance, RSC Adv. 6 (63) (2016) 58236–58246.
[89] T. Arfin, S.N. Rangari, Graphene oxide–ZnO nanocomposite modified electrode for the detection of phenol, Anal. Methods 10 (3) (2018) 347–358.
[90] M.M. Rahman, Selective and sensitive 4-Aminophenol chemical sensor development based on low-dimensional Ge-doped ZnO nanocomposites by electrochemical method, Microchem. J. 157 (2020), 104945.
[91] A. Wahid, A.M. Asiri, M.M. Rahman, One-step facile synthesis of Nd2O3/ZnO nanostructures for an efficient selective 2, 4-dinitrophenol sensor probe, Appl. Surf. Sci. 487 (2019) 1253–1261.
[92] R. Ahmad, N. Tripathy, M.S. Ahn, Y.B. Hahn, Highly stable hydrazine chemical sensor based on vertically-aligned ZnO nanorods grown on electrode, J. Colloid Interface Sci. 494 (2017) 153–158.
[93] M.M. Rahman, H.B. Balkhoyor, A.M. Asiri, Ultrasensitive and selective hydrazine sensor development based on Sn/ZnO nanoparticles, RSC Adv. 6 (35) (2016) 29342–29352.
[94] A.A. Ismail, F.A. Harraz, M. Faisal, A.M. El-Toni, A. Al-Hajry, M.S. Al-Assiri, A sensitive and selective amperometric hydrazine sensor based on mesoporous Au/ZnO nanocomposites, Mater. Design 109 (2016) 530–538.
[95] A. Umar, M.M. Rahman, Y.B. Hahn, Ultra-sensitive hydrazine chemical sensor based on high-aspect-ratio ZnO nanowires, Talanta 77 (4) (2009) 1376–1380.
[96] S.K. Mehta, K. Singh, A. Umar, G.R. Chaudhary, S. Singh, Ultra-high sensitive hydrazine chemical sensor based on low-temperature grown ZnO nanoparticles, Electrochim. Acta 69 (2012) 128–133.
[97] S. Kumar, G. Bhanjana, N. Dilbaghi, A. Umar, Zinc oxide nanocones as potential scaffold for the fabrication of ultra-high sensitive hydrazine chemical sensor, Ceram. Int. 41 (2) (2015) 3101–3108.
[98] M. Jang, D. Jung, J. Lee, S.M. Lee, A. Lee, S. Yim, K.S. An, PVDF-stimulated surface engineering in ZnO for highly sensitive and water-stable hydrazine sensors, Appl. Surf. Sci. (2022), 152747.
[99] A. Mousavi-Majd, S. Ghasemi, S.R. Hosseini, Zeolitic imidazolate framework derived porous ZnO/Co3O4 incorporated with gold nanoparticles as ternary nanohybrid for determination of hydrazine, J. Alloys Compd. 896 (2022), 162922.
[100] A.A. Ibrahim, G.N. Dar, S.A. Zaidi, A. Umar, M. Abaker, H. Bouzid, S. Baskoutas, Growth and properties of Ag-doped ZnO nanoflowers for highly sensitive phenyl hydrazine chemical sensor application, Talanta 93 (2012) 257–263.
[101] A. Umar, S.H. Kim, R. Kumar, M.S. Al-Assiri, A.E. Al-Salami, A.A. Ibrahim, S. Baskoutas, In-doped ZnO hexagonal stepped nanorods and nanodisks as potential scaffold for highly-sensitive phenyl hydrazine chemical sensors, Materials 10 (11) (2017) 1337.
[102] A.A. Ibrahim, P. Tiwari, M.S. Al-Assiri, A.E. Al-Salami, A. Umar, R. Kumar, S. Baskoutas, A highly-sensitive picric acid chemical sensor based on ZnO nanopeanuts, Materials 10 (7) (2017) 795.
[103] A. Mohammad, K. Ahmad, A. Qureshi, M. Tauqeer, S.M. Mobin, Zinc oxide-graphitic carbon nitride nanohybrid as an efficient electrochemical sensor and photocatalyst, Sens. Actuators B 277 (2018) 467–476.
[104] T. Yang, Y. Cui, M. Chen, R. Yu, S. Luo, W. Li, K. Jiao, Uniform and vertically oriented ZnO nanosheets based on thin-layered MoS2: synthesis and high-sensing ability, ACS Sustain. Chem. Eng. 5 (2) (2017) 1332–1338.
[105] Y. Wang, R. Xu, L. Chen, C. Wu, L. Qiu, C.D. Windle, L. Qu, Hierarchical ZnO@ hybrid carbon core–shell nanowire array on a graphene fiber microelectrode for ultrasensitive detection of 2, 4, 6-trinitrotoluene, ACS Appl. Mater. Interfaces 12 (7) (2020) 8547–8554.
[106] E.B. Kim, M. Imran, E.H. Lee, M.S. Akhtar, S. Ameen, Multiple ions detection by field-effect transistor sensors based on ZnO@ GO and ZnO@ rGO nanomaterials: Application to trace detection of Cr (III) and Cu (II), Chemosphere 286 (2022), 131695.
[107] V.H. Oliveira, F. Rechotnek, E.P. da Silva, V. de Sousa Marques, A.F. Rubira, R. Silva, E.C. Muniz, A sensitive electrochemical sensor for Pb2+ ions based on ZnO nanofibers functionalized by L-cysteine, J. Mol. Liq. 309 (2020), 113041.
[108] A. Moutcine, C. Laghlimi, Y. Ziat, M.A. Smaini, S.E. El Qouatli, M. Hammi, A. Chtaini, Preparation, characterization and simultaneous electrochemical detection toward Cd (II) and Hg (II) of a phosphate/zinc oxide modified carbon paste electrode, Inorg. Chem. Commun. 116 (2020), 107911.
[109] R. Karthik, S. Thambidurai, Synthesis of cobalt doped ZnO/reduced graphene oxide nanorods as active material for heavy metal ions sensor and antibacterial activity, J. Alloys Compd. 715 (2017) 254–265.
[110] E.B. Kim, M. Imran, E.H. Lee, M.S. Akhtar, S. Ameen, Multiple ions detection by field-effect transistor sensors based on ZnO@ GO and ZnO@ rGO nanomaterials: Application to trace detection of Cr (III) and Cu (II), Chemosphere 286 (2022), 131695.
[111] S. Pitchaiya, M. Natarajan, A. Santhanam, V. Asokan, A. Yuvapragasam, V. M. Ramakrishnan, D. Velauthapillai, A review on the classification of organic/inorganic/carbonaceous hole transporting materials for perovskite solar cell application, Arabian J. Chem. 13 (1) (2020) 2526–2557.
[112] M.F. Soh, M.F.M. Noh, N.A. Mohamed, J. Safaei, N.N. Rosli, E.L. Lim, M.A. M. Teridi, Incorporation of g-C3N4/Ag dopant in TiO2 as electron transport layer for organic solar cells, Mater. Lett. 253 (2019) 117–120.
[113] Y. Xiao, N. Cheng, K.K. Kondamareddy, C. Wang, P. Liu, S. Guo, X.Z. Zhao, W-doped TiO2 mesoporous electron transport layer for efficient hole transport material free perovskite solar cells employing carbon counter electrodes, J. Power Sources 342 (2017) 489–494.
[114] G. Yang, P. Qin, G. Fang, G. Li, Tin oxide (SnO2) as effective electron selective layer material in hybrid organic–inorganic metal halide perovskite solar cells, J. Energy Chem. 27 (4) (2018) 962–970.
[115] Y. Li, H.Q. Wang, H. Zhou, D. Du, W. Geng, D. Lin, J. Kang, Tuning the surface morphologies and properties of ZnO films by the design of interfacial layer, Nanoscale Res. Lett. 12 (1) (2017) 1–7.
[116] Y.M. Sung, A.K. Akbar, S. Biring, C.F. Li, Y.C. Huang, S.W. Liu, The effect of ZnO preparation on the performance of inverted polymer solar cells under one sun and indoor light, J. Mater. Chem. C 9 (4) (2021) 1196–1204.
[117] Y. Xiong, M. Fang, Q. Zhang, W. Liu, X. Liu, L. Ma, X. Xu, Reproducible and arbitrary patterning of transparent ZnO nanorod arrays for optic and biomedical device integration, J. Alloys Compd. 898 (2022), 163003.
[118] D.Y. Son, J.H. Im, H.S. Kim, N.G. Park, 11% efficient perovskite solar cell based on ZnO nanorods: an effective charge collection system, J. Phys. Chem. C 118 (30) (2014) 16567–16573.
[119] K. Mahmood, B.S. Swain, A. Amassian, 16.1% efficient hysteresis-free mesostructured perovskite solar cells based on synergistically improved ZnO nanorod arrays, Adv. Energy Mater. 5 (17) (2015), 1500568.
[120] J. Song, L. Liu, X.F. Wang, G. Chen, W. Tian, T. Miyasaka, Highly efficient and stable low-temperature processed ZnO solar cells with triple cation perovskite absorber, J. Mater. Chem. A 5 (26) (2017) 13439–13447.
[121] S. Hernández, D. Hidalgo, A. Sacco, A. Chiodoni, A. Lamberti, V. Cauda, G. Saracco, Comparison of photocatalytic and transport properties of TiO 2 and ZnO nanostructures for solar-driven water splitting, Phys. Chem. Chem. Phys. 17 (12) (2015) 7775–7786.
[122] R.A.A. Madlol, Structural and optical properties of ZnO nanotube synthesis via novel method, Results Phys. 7 (2017) 1498–1503.
[123] B. Liu, H.C. Zeng, Hydrothermal synthesis of ZnO nanorods in the diameter regime of 50 nm, J. Am. Chem. Soc. 125 (15) (2003) 4430–4431.
[124] S.N. Kwon, J.H. Yu, S.I. Na, A systematic approach to ZnO nanoparticle-assisted electron transport bilayer for high efficiency and stable perovskite solar cells, J. Alloys Compd. 801 (2019) 277–284.
[125] N. Islavath, G. Lingamallu, The performance enhancement of HTM-free ZnO nanowire-based perovskite solar cells via low-temperature TiCl4 treatment, Sol. Energy 170 (2018) 158–163.
[126] M. Hong, J. Meng, H. Yu, J. Du, Y. Ou, Q. Liao, Y. Zhang, Ultra-stable ZnO nanobelts in electrochemical environments, Mater. Chem. Front. 5 (1) (2021) 430–437.
[127] K. Mahmood, A. Khalid, Single-step electrospray deposited nitrogen-doped ZnO nanosheets yield hysteresis-free perovskite solar cells, Mater. Lett. 224 (2018) 78–81.
[128] M. Bidikoudi, E. Kymakis, Novel approaches and scalability prospects of copper based hole transporting materials for planar perovskite solar cells, J. Mater. Chem. C 7 (44) (2019) 13680–13708.
[129] D. Liu, T.L. Kelly, Perovskite solar cells with a planar heterojunction structure prepared using room-temperature solution processing techniques, Nat. Photonics 8 (2) (2014) 133–138.
[130] J. Kim, G. Kim, T.K. Kim, S. Kwon, H. Back, J. Lee, K. Lee, Efficient planar-heterojunction perovskite solar cells achieved via interfacial modification of a sol–gel ZnO electron collection layer, J. Mater. Chem. A 2 (41) (2014) 17291–17296.
[131] A. Naveed Ul Haq, A. Nadhman, I. Ullah, G. Mustafa, M. Yasinzai, I. Khan, Synthesis approaches of zinc oxide nanoparticles: the dilemma of ecotoxicity, J. Nanomater. 2017 (2017).
[132] Z.L. Tseng, C.H. Chiang, C.G. Wu, Surface engineering of ZnO thin film for high efficiency planar perovskite solar cells, Sci. Rep. 5 (1) (2015) 1–10.
[133] X. Dong, H. Hu, B. Lin, J. Ding, N. Yuan, The effect of ALD-Zno layers on the formation of CH 3 NH 3 PbI 3 with different perovskite precursors and sintering temperatures, Chem. Commun. 50 (92) (2014) 14405–14408.
[134] S.S. Shin, S.J. Lee, S.I. Seok, Exploring wide bandgap metal oxides for perovskite solar cells, APL Mater. 7 (2) (2019), 022401.
[135] D.Y. Son, K.H. Bae, H.S. Kim, N.G. Park, Effects of seed layer on growth of ZnO nanorod and performance of perovskite solar cell, J. Phys. Chem. C 119 (19) (2015) 10321–10328.
[136] M.S. Selim, A.M. Elseman, Z. Hao, ZnO nanorods: an advanced cathode buffer layer for inverted perovskite solar cells, ACS Appl. Energy Mater. 3 (12) (2020) 11781–11791.
[137] J. Zhang, P. Barboux, T. Pauporté, Electrochemical design of nanostructured ZnO charge carrier layers for efficient solid-state perovskite-sensitized solar cells, Adv. Energy Mater. 4 (18) (2014), 1400932.
[138] K. Mahmood, B.S. Swain, H.S. Jung, Controlling the surface nanostructure of ZnO and Al-doped ZnO thin films using electrostatic spraying for their application in 12% efficient perovskite solar cells, Nanoscale 6 (15) (2014) 9127–9138.
[139] N. Li, F. Meng, F. Huang, G. Yu, Z. Wang, J. Yan, J. Ye, Room-temperature sputtered aluminum-doped zinc oxide for semitransparent perovskite solar cells, ACS Appl. Energy Mater. 3 (10) (2020) 9610–9617.
[140] J. Dong, Y. Zhao, J. Shi, H. Wei, J. Xiao, X. Xu, Q. Meng, Impressive enhancement in the cell performance of ZnO nanorod-based perovskite solar cells with Al-doped ZnO interfacial modification, Chem. Commun. 50 (87) (2014) 13381–13384.
[141] J. Dong, J. Shi, D. Li, Y. Luo, Q. Meng, Controlling the conduction band offset for highly efficient ZnO nanorods based perovskite solar cell, Appl. Phys. Lett. 107 (7) (2015), 073507.

[142] Y.Z. Zheng, E.F. Zhao, F.L. Meng, X.S. Lai, X.M. Dong, J.J. Wu, X. Tao, Iodine-doped ZnO nanopillar arrays for perovskite solar cells with high efficiency up to 18.24%, J. Mater. Chem. A 5 (24) (2017) 12416–12425.
[143] T. Wu, Z. Qin, Y. Wang, Y. Wu, W. Chen, S. Zhang, L. Han, The Main Progress of Perovskite Solar Cells in 2020–2021, Nano-Micro Lett. 13 (1) (2021) 1–18.
[144] C. Liu, W. Wu, D. Zhang, Z. Li, G. Ren, W. Han, W. Guo, Effective stability enhancement in ZnO-based perovskite solar cells by MACl modification, J. Mater. Chem. A 9 (20) (2021) 12161–12168.
[145] C.L. Hsu, E.C. Chang, H.T. Hsueh, Y.H. Liu, Solution-synthesized p-type CuMnO2 and n-type ZnO to form the core-shell nanowires for photo and gas sensing, J. Alloys Compd. 899 (2022), 163380.
[146] S. Angaiah, S. Arunachalam, V. Murugadoss, G. Vijayakumar, A facile polyvinylpyrrolidone assisted solvothermal synthesis of zinc oxide nanowires and nanoparticles and their influence on the photovoltaic performance of dye sensitized solar cell, ES Energy Environ. 4 (3) (2019) 59–65.
[147] S.R. Bhattacharyya, Z. Mallick, R.N. Gayen, Vertically aligned Al-doped ZnO nanowire arrays as efficient photoanode for dye-sensitized solar cells, J. Electron. Mater. 49 (6) (2020).
[148] Q. Hu, Y. Li, F. Huang, Z. Zhang, K. Ding, M. Wei, Z. Lin, ZnO nanowires array grown on Ga-doped ZnO single crystal for dye-sensitized solar cells, Sci. Rep. 5 (1) (2015) 1–7.
[149] C.Y. Jiang, X.W. Sun, G.Q. Lo, D.L. Kwong, J.X. Wang, Improved dye-sensitized solar cells with a ZnO-nanoflower photoanode, Appl. Phys. Lett. 90 (26) (2007), 263501.
[150] M. Law, L.E. Greene, A. Radenovic, T. Kuykendall, J. Liphardt, P. Yang, ZnO− Al2O3 and ZnO− TiO2 core− shell nanowire dye-sensitized solar cells, J. Phys. Chem. B 110 (45) (2006) 22652–22663.
[151] C. Xu, J. Wu, U.V. Desai, D. Gao, High-efficiency solid-state dye-sensitized solar cells based on TiO2-coated ZnO nanowire arrays, Nano Lett. 12 (5) (2012) 2420–2424.
[152] C.S. Chou, F.C. Chou, J.Y. Kang, Preparation of ZnO-coated TiO2 electrodes using dip coating and their applications in dye-sensitized solar cells, Powder Technol. 215 (2012) 38–45.
[153] Z. Li, W. Liu, R. Wang, F. Chen, J. Chen, Y. Zhu, C. Xu, Interface design for electrically pumped ultraviolet nanolaser from single ZnO-nanorod, Nano Energy 93 (2022), 106832.
[154] A. Rakhsha, H. Abdizadeh, E. Pourshaban, M.R. Golobostanfard, M. Montazerian, V.R. Mastelaro, Controlling the performance of one-dimensional homojunction UV detectors based on ZnO nanoneedles array, Sens. Actuators A (2021), 112916.
[155] C. Li, X. Fan, L. Yu, L. Cui, M. Yin, Y. Li, N. Liu, A resistive-type UV detector based on ZnO nanowalls decoated by Ag nanowires, Opt. Mater. 103 (2020), 109891.
[156] S. Singh, S.H. Park, Fabrication and properties of ZnO nanorods based MSM UV detectors on silicon substrates, Optik 137 (2017) 96–100.
[157] T.H. Eom, J.I. Han, Single fiber UV detector based on hydrothermally synthesized ZnO nanorods for wearable computing devices, Appl. Surf. Sci. 428 (2018) 233–241.
[158] L. Guo, H. Zhang, D. Zhao, B. Li, Z. Zhang, M. Jiang, D. Shen, High responsivity ZnO nanowires based UV detector fabricated by the dielectrophoresis method, Sens. Actuators B 166 (2012) 12–16.
[159] J.P. Kar, S.N. Das, J.H. Choi, Y.A. Lee, T.Y. Lee, J.M. Myoung, Fabrication of UV detectors based on ZnO nanowires using silicon microchannel, J. Cryst. Growth 311 (12) (2009) 3305–3309.
[160] N. Nasiri, R. Bo, F. Wang, L. Fu, A. Tricoli, Ultraporous electron-depleted ZnO nanoparticle networks for highly sensitive portable visible-blind UV photodetectors, Adv. Mater. 27 (29) (2015) 4336–4343.
[161] S.M. Mohammad, S. Rajamanickam, Z. Hassan, M. Abdullah, A.R. Shafiqa, A. Abuelsamen, Self-powered UV photodetector performance optimization based on Ag nanoparticles-encapsulated-ZnO nanorods by photo-deposition method, Sens. Actuators A 331 (2021), 113032.
[162] F. Abbasi, F. Zahedi, M. hasan Yousefi, Fabricating and investigating high photoresponse UV photodetector based on Ni-doped ZnO nanostructures, Optics Commun. 482 (2021), 126565.
[163] Y. Liu, Z. Song, M. Hu, J. Chen, S. Yuan, L. Xu, Self-powered adjustable UV and NIR photodetectors based on one-step synthesized TeO2 doped ZnO composite nanorods/Si heterojunction, Sens. Actuators A 331 (2021), 113009.
[164] P. Sahatiya, S.S. Jones, V. Mattela, S. Badhulika, Direct growth of black phosphorus (p-type) on a flexible substrate with dual role of two-dimensional ZnO (n-type) as effective passivation and enabling highly stable broadband photodetection, ACS Appl. Electron. Mater. 1 (7) (2019) 1076–1083.
[165] P. Sahatiya, S.S. Jones, P.T. Gomathi, S. Badhulika, Flexible substrate based 2D ZnO (n)/graphene (p) rectifying junction as enhanced broadband photodetector using strain modulation, 2D Mater. 4 (2) (2017), 025053.